# Orientation Dynamics of Anisotropic Particles in Viscoelastic Fluids

A Thesis

Submitted for the Degree of

MASTER OF SCIENCE (ENGINEERING)

in the Faculty of Engineering

by

VIVEKANAND DABADE


ENGINEERING MECHANICS UNIT
JAWAHARLAL NEHRU CENTRE FOR ADVANCED SCIENTIFIC RESEARCH
(A Deemed University)
Bangalore – 560 064

APRIL 2009

## DECLARATION

I hereby declare that the matter embodied in the thesis entitled "**Orientation Dynamics of Anisotropic Particles in Viscoelastic Fluids**" is the result of investigations carried out by me at the Engineering Mechanics Unit, Jawaharlal Nehru Centre for Advanced Scientific Research, Bangalore, India under the supervision of Dr. Ganesh Subramanian and that it has not been submitted elsewhere for the award of any degree or diploma.

In keeping with the general practice in reporting scientific observations, due acknowledgment has been made whenever the work described is based on the findings of other investigators.

Vivekanand Dabade

## CERTIFICATE

I hereby certify that the matter embodied in this thesis entitled "**Orientation Dynamics of Anisotropic Particles in Viscoelastic Fluids**" has been carried out by Mr. Vivekanand Dabade at the Engineering Mechanics Unit, Jawaharlal Nehru Centre for Advanced Scientific Research, Bangalore, India under my supervision and that it has not been submitted elsewhere for the award of any degree or diploma.

Dr. Ganesh Subramanian
(Research Supervisor)

# Acknowledgements

First and foremost I would like to thank my research adviser, Dr. Ganesh Subramanian, for suggesting the problem and showing keen interest during all the stages of the project. His unique physical insights towards problem solving and unwavering enthusiasm for research will always be a great source of inspiration for me. I am grateful for his patience and the faith he showed in me during the entire project.

I would like to acknowledge Prof. K. R. Sreenivas for providing me financial support during the final stages of this project, Mukund for being a great friend whose diverse interests have always amazed me and my colleagues: Anubhab, Sumesh, Harish, Rakshith, Ratul, Ponnu, Aditya, Gayathri and Rahul for providing a congenial atmosphere in the lab. I would like to express my gratitude to Rinki and her labmates for making my stay at the hostel an enjoyable one. Outside JNC, I would like to thank Sasi, Sourabh, Bhavani, Sridhar, Shankar and Varun for being great friends, the best I could have asked for.

Most of all, I would like to express my love and gratitude to my parents and sister for supporting and encouraging me in all the endeavours I have taken up so far.

# Contents

# Abstract

The present work concerns the orientation dynamics of anisotropic particles in viscoelastic fluids. A spheroidal geometry is taken as being representative of an anisotropic, axisymmetric particle, and the work is an analytical investigation of the effects of weak inertia and viscoelasticity on the orientation of a spheroidal particle (both prolate and oblate) of an arbitrary aspect ratio in two canonical flow situations:
1. A spheroid sedimenting in a quiescent fluid, and
2. A neutrally buoyant spheroid in a simple shear flow
Applications include sedimentation of muds and slurries, processing of cellulose fiber suspensions in the paper and pulp industry, and processing of filled polymeric materials (wherein anisotropic clay particles are typically used as cheap filler materials).

In the absence of both inertia and viscoelasticity, the orientation dynamics of a spheroid is governed by the Stokes equations. On account of reversibility, a sedimenting spheroid continues to retain its initial orientation, while a neutrally buoyant spheroid in simple shear continues to rotate in an initially chosen (Jeffery) orbit. In either case, the particle orientation distribution remains indeterminate as a result. In situations where the characteristics of the motion of a single anisotropic particle may be applied to the calculation of a bulk property of a dilute non-interacting suspension of such particles, the aforementioned indeterminacy in the orientation distribution presents an impediment. In order to eliminate the indeterminacy, and thereby, arrive at a unique orientation distribution, it becomes necessary to consider the influence of additional physical phenomena. Possible candidates for the resolution of the indeterminacy include Brownian motion, pair-particle hydrodynamic interactions, fluid inertia, viscoelasticity of the suspending fluid, etc.

The present work focuses on weak fluid inertia and viscoelasticity with a weakly

viscoelastic fluid being modeled as a second-order fluid in the analysis. It is important to note here that even a weak deviation from the Stokes limit will invariably have a strong cumulative effect over long times precisely due to the above indeterminacy. For instance, a weak inertial torque, acting on a sedimenting spheroid, stabilizes orientations transverse to gravity, while a weak viscoelastic torque ends up stabilizing the longitudinal (vertical) orientation. In both cases, the indeterminacy in the orientation distribution is eliminated. One anticipates a similar situation for the case of simple shear flow.

The canonical motions of a spheroid referred to above, sedimentation in particular, are classic problems, and have been extensively investigated, both theoretically and experimentally, by various authors. The present work analyzes both problems using a new approach based on the formalism of vectorial spheroidal harmonics. The formalism was developed by Vladimir Kushch [see Kushch & Sangani (2003)] and has a structure similar to the well-known spherical harmonics formalism which owes its origin to Lamb (1932). Unlike earlier approaches, and in a manner similar to spherical harmonics, the spheroidal harmonics formalism is readily extended to a multi-particle scenario wherein hydrodynamic interactions between anisotropic particles may begin to play an important role in determining the orientation dynamics. However, as a first step, in this work, the formalism is applied to the motion of a single particle, and the results obtained compared to those of earlier investigations.

The formalism, together with the use of the generalized reciprocal theorem, is first applied to the sedimentation problem, leading to closed-form analytical expressions for the $O(Re)$ inertial and $O(De)$ viscoelastic torques in both sedimentation and simple shear flow as a function of the spheroid aspect ratio. Here, the Reynolds number and the Deborah number denote the scaled magnitudes of the inertial and viscoelastic torques, respectively. Since the two torques act in opposite directions, a balance of the two leads to a neutral curve, that is, a critical value of De/Re as a function of the particle aspect ratio [see figures 3.13 & 3.15] that separates regions where transverse and longitudinal orientations are stable. Despite extensive work on this classic problem, our fully analytical approach shows some of the earlier results to be incorrect. In particular, it is shown that the viscoelastic torque always tends to zero in the limit of an infinitely slender particle for an arbitrary ratio of the two normal stress differences [see §3.2.1]. In fact, the viscoelastic torque be-

comes extremely sensitive to changes in the particle aspect ratio in the limit of very slender particles, and this may be one reason why earlier numerical calculations of the same turn out to be erroneous [see §3.2.1].

The inertial and viscoelastic contributions to the angular velocity of a neutrally buoyant spheroid in simple shear flow are currently being calculated. The simple shear flow problem is inherently more complicated, since the orientation of the spheroid now changes as a function of time even in the inertialess limit (as the particle moves along a Jeffery orbit) [see Jeffery (1922)]. Further, unlike sedimentation where the only stable orientations turn out to the transverse and longitudinal ones, the more complicated angular dependencies in simple shear flow allow, in principle, for the existence of stable intermediate orbits (that is, in between the limits of in-plane tumbling and log-rolling). Significant progress has already been made, and in the near future, we expect to be able to map out the orientation dynamics in presence of the (possibly) competing effects of viscoelasticity and inertia. Our aim then is to obtain an orbit-constant-surface as a function of De/Re and the particle aspect ratio [see figure 4.1].

# List of Figures

# List of Tables

CHAPTER 1

# INTRODUCTION

A suspension is a dispersion of solid particles in a fluid medium. Solid particles constituting the disperse phase, are suspended in a continuous phase which is a liquid or a gas. Suspensions typically possess a definite small-scale structure (the disperse phase constituents or particles) that is much larger than the atomic or molecular scale. This usually is referred to as the microstructure. This is unlike simple fluids like air, water or honey which are composed of atomic constituents, and hence may be regarded as structure-less. On length scales larger than the atomic, the motion of simple fluids is governed by the Navier-Stokes equations.

Suspensions can be found readily in our everyday lives. Chocolates are concentrated suspension of sugar crystals, cocoa and milk solids in a continuous fat matrix. Ice-cream is a suspension of microscopic ice crystals dispersed in cream. Blood, the most common biological fluid, is a concentrated suspension of red blood cells (bi-concave disks), white blood cells (irregularly shaped particles) and platelets in a plasma medium.

Suspensions find immense applications in industry as well. For example, in the paper-pulp industry, paper manufacture involves the processing of cellulose fiber suspensions in an aqueous medium and the orientation distribution of fibers under flow conditions decides, in part, the characteristics of the final product. Nanoparticle suspensions, popularly known as nanofluids, are being touted as the future heat-transfer agents. The addition of short fiber-like particles to a polymer matrix

is known to enhance the mechanical properties of the resulting composite material, and the degree of enhancement depends strongly on the orientation of the fibers. The fiber orientation is caused by the flow occurring in the molten state.

The inherent complexity of these fascinating fluids, and their ubiquity evident from their wide-ranging applications, and presence in our daily life and industry, makes the study of suspensions of great interest and importance. This thesis examines the orientation dynamics of axisymmetric (spheroidal) particles in sedimentation and simple shear flow.

## 1.1 Literature Survey

Suspensions of spherical particles have been studied in this regard [see Kim & Karrila (1991)], Batchelor (1972), for instance determined the average sedimentation velocity in a dilute homogenous suspension arising from pair-particle interactions. There are significant differences between sedimenting suspensions of spherical and anisotropic particles. In the latter case, Koch & Shaqfeh (1989) showed that a dilute suspension of spheroids is unstable to number density fluctuations in the inertialess limit. Factors such as inertia and viscoelasticity even in small amounts may play a crucial role in stabilizing such a suspension.

### Review of experimental work

The case of single particle sedimentation in a quiescent fluid is a logical first step in understanding the dynamics of a dilute sedimenting suspension.

In the absence of both inertia and viscoelasticity, the orientation dynamics of a spheroid is governed by the Stokes equations. Using reversibility arguments, one can show that a sedimenting spheroid continues to retain its initial orientation.

This may be seen from the photograph of an experiment performed by Leal (1975), in which the motion of slender particles in a highly viscous fluid is studied [See figure 1.1(a)]. Leal (1975) also carried out preliminary experimental investigations on the motion of cylindrical particles with rounded ends (slender particles) in 0.5% Dow's Separan-AP30 (viscosity$\sim$ 0.15 Pa-sec), a viscoelastic fluid, and in 99.5% glycerine solution (viscosity$\sim$ 1.150 Pa-sec), a Newtonian fluid. The cylindrical particle (0.704in in length and axis ratio of 28) was introduced into the top of the tank (18 in. in height and 6 in. square in cross-section) and observations were made by taking successive photographs that were separated by a known increment of time.

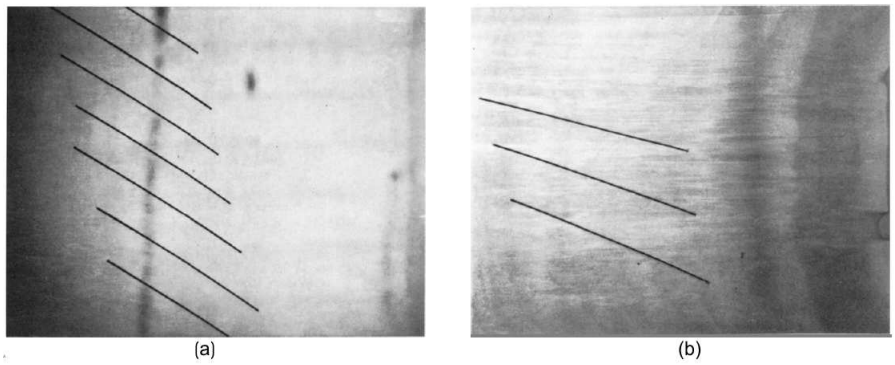


Figure 1.1: Leal(1975) Multiple-image photograph of a slender rod-like particle sedimenting in (a)Newtonian fluid, 99.5% glycerine (b)Viscoelastic fluid,0.5% Separan AP30,

The particle motion in Separan AP30 was markedly different from that in the 99.5% glycerine solution. The particles rotated rapidly from their initial orientation to a vertical orientation when sedimenting through the Separan-AP30 solution while the particle did not change its orientation in 99.5% glycerine solution.The photographs (figure1.1) show the results obtained.

Experiments performed by K.Chiba *et al.* (1986) demonstrated the effect of

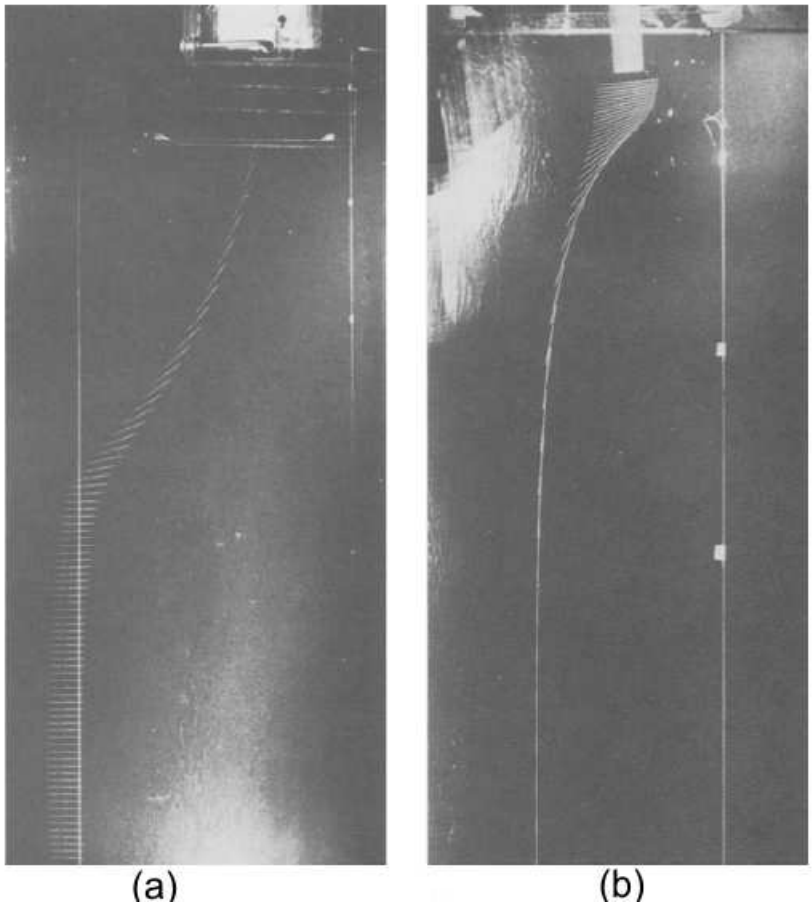


Figure 1.2: Chiba(1986) Multiflash photograph of slender body motion (a)Newtonian fluid,water (b)Viscoelastic fluid,0.25% by wt. Separan AP30 solution

inertia, which was not captured by Leal's experiments [see Leal (1975)]. Inertial effects were enhanced by using water as the suspending fluid. Slender bodies with a diameter 0.512mm diameter and a length of 60mm, were dropped in water and Separan AP-30 solution (0.5% concentration and having a viscosity of around 0.15 Pa-sec). The results obtained from the experiments may be seen from the multi-flash photographs tracking the body trajectory [see figure1.2]. The slender particle orients vertically in the viscoelastic fluid (Separan AP-30 solution) and adopts a horizontal position in the low viscosity Newtonian fluid (water).

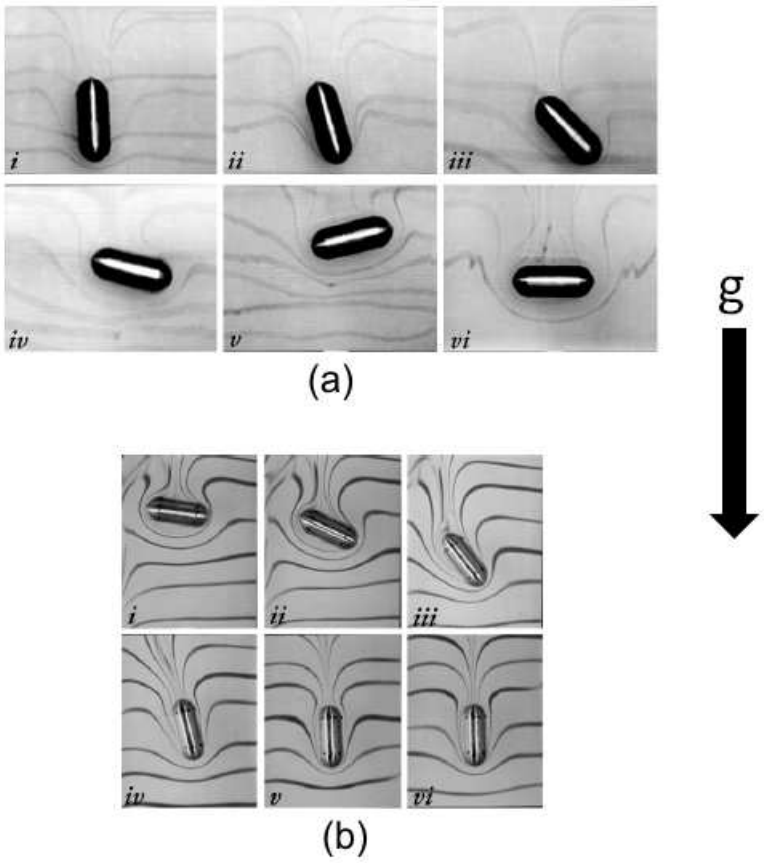


Figure 1.3: Galdi *et al.*(2002) Orientation of cylinders with rounded ends in (a)In the Newtonian case (b)purely viscoelastic liquid at vanishingly small Reynolds number

G.P.Galdi *et al.* (2002) obtained similar results in their experiments using cylinders with rounded ends. They concluded that the only possible equilibrium orientations are when the axis of the cylinder is either parallel or perpendicular to the acceleration due to gravity. Their results may be seen from figure1.3.

Experiments have also been conducted to study the motion of neutrally buoyant axisymmetric particles suspended in a simple shear flow. The motion of a single, small, neutrally buoyant particle suspended in a fluid which is undergoing simple shear flow ( $\boldsymbol{u}=\dot{\gamma}\mathrm{y}\boldsymbol{e}_x$, where $x$ is the flow direction, $y$ is the velocity gradient

direction, $z$ is the vorticity direction and $\dot{\gamma}$ is the shear rate [see figure 1.4]) has, in fact been the subject of a considerable number of theoretical and experimental investigations spanning approximately fifty years. Interest in this problem stems mainly from its central role in the determination of the bulk properties of a dilute suspension. Jeffery was the first to show that, an axisymmetric particle, suspended in a Newtonian fluid undergoing a simple shear flow, in the absence of inertia, may rotate in any one of an infinite number of orbits known as the Jeffery orbits [see Jeffery (1922)]. The particle executes a periodic orbiting motion which depends on its aspect ratio and the initial inclination. For a spheroidal particle in particular, the motion of the axis of symmetry of the particle is described by:

$$\begin{aligned} \frac{d\phi}{dt} &= \frac{\dot{\gamma}}{{A_r}^2+1}({A_r}^2\cos^2\phi+\sin^2\theta), \\ \frac{d\theta}{dt} &= \frac{\dot{\gamma}}{4}\left(\frac{{A_r}^2-1}{{A_r}^2+1}\right)\sin 2\theta\sin 2\phi, \end{aligned} \tag{1.1}$$

where $\dot{\gamma}$ is the shear rate, $\theta$ and $\phi$ are the polar and azimuthal angle respectively, as shown in the figure 1.4. Here, $A_r$ is the aspect ratio of the spheroidal particle or the ratio of the major and minor axes ($A_r > 1$ for a prolate spheroid and $A_r < 1$ for an oblate spheroid).

The equations of motion can be obtained in terms of the orbit constant $C$ by transforming coordinates from $(\theta, \phi)$ to $(C,\tau)$ in equation (1.1) using the transformation:

$$\theta = \tan^{-1}(C\sqrt{\cos^2\tau+{A_r}^2\sin^2\tau}),$$

$$\phi = \tan^{-1}(A_r\tan\tau). \tag{1.2}$$

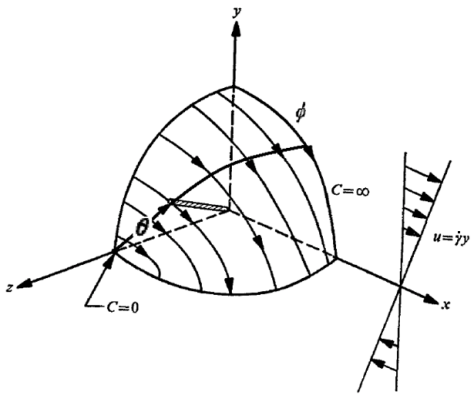


Figure 1.4: Jeffery orbits of an arbitrary aspect ratio prolate spheroid; the orbits are stretched along the flow direction. Whereas for an oblate spheroid, the Jeffery orbits would be stretched along the flow-gradient direction.

In this new coordinate system the equations of motion become:

$$\frac{dC}{dt} = 0, \tag{1.3}$$

$$\frac{d\tau}{dt} = \frac{A_r\dot{\gamma}}{{A_r}^2 + 1},$$

where $C$ is the orbit constant, and can vary from 0 (corresponding to a log-rolling motion about the vorticity axis) to $\infty$ (corresponding to a tumbling motion in the plane of shear); $\tau$ indicates the phase of the particle in the orbit. Equation (1.3) shows that the orbit constant $C$ does not vary with time, and the particle therefore continues to remain in the orbit which it was initially in.

Mason and his co-workers [see Bartman *et al.* (1975)] reported the effect of inertia and viscoelasticity of the fluid on the orbit of a rotating particle in a simple shear flow. They studied the motion of nylon rods (aspect ratio$\geq$10) and polystyrene discs (aspect ratio$\approx$0.1) in the annulus between counter-rotating cylinders of a Couette apparatus. 2.5% polyacrylamide in water was used as a viscoelastic fluid (viscosity$\sim$ 0.7 Pa-sec) and Glycerol (viscosity$\sim$ 0.6 Pa-sec) was used as a New-

tonian fluid. Their experiments conclusively showed that the effect of inertia was to cause rods and disks to gradually drift into orbits of maximum dissipation; that is, the rods drift to C=$\infty$, where they rotate completely in the plane of the flow (tumbling motion), and the disks drift to C=0 where they spin (log-rolling motion) with the axis of symmetry aligned with the vorticity vector of the undisturbed flow. On the other hand, at low shear rates, viscoelasticity causes the particle to drift into orbits of minimum dissipation, exactly the opposite of what inertia would do.

## Review of analytical and computational work

The effects of inertia and viscoelasticity on the motion of axisymmetric particles, in the context of both sedimentation and shear, have been studied with great interest owing to the interesting phenomena revealed by experiments described in the earlier section. Many authors have analysed this problem both numerically and analytically.

Cox (1965) found an analytical expression for the inertial torque to $O(Re)$ on a spheroid of small eccentricity using the method of asymptotic expansions. The Reynolds number is defined as $Re = \frac{\rho UL}{\mu}$, where $\rho$ is the density of the fluid, $U$ is the velocity of translation of the spheroid, $L$ is the major diameter of the spheroid and $\mu$ is the viscosity of the fluid. He assumed the body surface to have the (dimensionless) form

$r = 1 + \epsilon \left\{ r^3 \frac{\partial^2}{\partial r_1^2}\left(\frac{1}{r}\right) \right\}$

using rectangular Cartesian co-ordinates $(r_1, r_2, r_3)$ with the origin fixed in the body. The term $(r^3 \frac{\partial^2}{\partial r_1^2}(\frac{1}{r}))$ is a surface harmonic of order two and $\epsilon$ is a dimensionless measure of the departure from sphericity. The parameter $\epsilon$ is assumed small so that squares and higher-order terms were neglected. The surface to $O(\epsilon)$ is a

spheroid axially symmetric about the direction 1 ($\epsilon > 0$ for a prolate spheroid and $\epsilon < 0$ for an oblate spheroid). The $O(Re)$ inertial torque $\boldsymbol{L_{sed(inertial)}}$ was found to be:

$$\boldsymbol{L_{sed(inertial)}} = Re\frac{29\pi}{40}\epsilon\mu UL^2 \sin 2\alpha \tag{1.4}$$

where U is the velocity of the body, $\rho$ is the density of the fluid, $\mu$ is the viscosity of the fluid, L is the length of the body and $\alpha$ being the angle between the translational velocity and axis of symmetry. In our notation $\epsilon$ is defined as: $\epsilon{=}\frac{1}{2\xi_0^2}$, here $\xi_0$ represents the surface of the particle in spheroidal coordinates, further details about our notation can be found in §2.1.1 of the second chapter. The sense of the inertial torque is so as to make the axis of symmetry perpendicular to the velocity of translation.

Later, Khayat and Cox (1989) derived an expression for the inertial torque, for finite $Re$, on a sedimenting fiber of large aspect ratio using slender body theory [see Batchelor (1970) & Cox (1970)]. The inertial torque again makes the particle eventually sediment with its centerline perpendicular to its direction of translation. The torque acting on the slender fiber in the limit $Re << 1$ is given by:

$$\boldsymbol{L_{sed(inertial)}} = Re\frac{-5\pi}{6\left(ln(A_r)\right)^2}\mu UL^2 \sin 2\alpha \tag{1.5}$$

where $\alpha$ is the angle the axis of the fiber makes with the translation velocity and $A_r$ is the aspect ratio of the particle.

On the other hand, the effect of viscoelasticity on a fiber sedimenting in a second order fluid was first determined by Leal (1975) again using slender body theory. The viscoelastic fluid in the theoretical analysis was modelled as a second-order fluid. His analysis showed that the viscoelastic torque rotates the axis of the

slender fiber towards alignment with the direction of translation. In particular, the expression for the viscoelastic torque acting on the slender fiber was given by:

$$\boldsymbol{L_{sed(visco)}} = De\frac{-\pi}{36}(16 - 96\epsilon_1)\mu U L^2 \sin 2\alpha \tag{1.6}$$

where $\epsilon_1$ is related to the ratio of the normal stress coefficients of the second-order fluid. $\epsilon_1$ is defined as $\frac{-\boldsymbol{\psi_1}}{2(\boldsymbol{\psi_1}+\boldsymbol{\psi_2})}$ and is therefore a material property. $\psi_1$ and $\psi_2$ can be defined in terms of the familiar normal stress differences, $N_1$ and $N_2$, as: $\psi_1{=}\frac{N_1}{\dot{\gamma}^2}$ and $\psi_2{=}\frac{N_2}{\dot{\gamma}^2}$ [see Larson (1988)]. Here Deborah number is defined as $De = \frac{\lambda U}{L}$, $\lambda$ is the intrinsic relaxation time of the second-order fluid.

Feng *et al.* (1995) solved the problem of a sedimenting spheroid numerically on a three-dimensional domain using a finite element method with fictitious domains. They reported the existence of equilibrium tilt angles between zero and ninety degrees that the settling prolate spheroid would eventually assume. In a more recent work, G.P.Galdi *et al.* (2002) determined the inertial and viscoelastic torques, semi-analytically, on a prolate spheroidal particle of an arbitrary aspect ratio. They used the singularity method for Stokes flows, originally developed by Chwang and Wu [see T.Chwang & Wu (1974) and Chwang & Wu (1975)], to obtain the disturbance velocity field due to a translating prolate spheroid. Although, closed form analytical expressions for the velocity fields were used, the final integration for the torque was carried out using a numerical integration package. They showed that only transverse and longitudinal equilibrium orientations are possible. Shatz (2004) has since extended the singularity method to the case of oblate spheroids by placing the fundamental singularities along an imaginary focal length. But, so far no literature has been found for the inertial and viscoelastic torques on an oblate spheroid of an arbitrary aspect ratio, sedimenting in a quiescent fluid.

In summary, the theoretical analyses for a sedimenting axisymmetric particle are in qualitative agreement with the experimental observations.

A large body of work exists on the problem of a spheroidal particle rotating in a simple shear flow. Jeffery (1922) showed that an axisymmetric particle, suspended in a Newtonian fluid undergoing a simple shear flow, may rotate in any one of an infinite number of orbits known as the Jeffery orbits in the absence of inertia. The effects of inertia on fiber motion in a simple shear flow have been examined in Subramanian & Koch (2005). It is shown therein that for small Reynolds number, the rotating fiber drifts toward the shearing plane and for Reynolds above a critical value the fiber ceases to rotate, instead drifting monotonically towards the shearing plane; in simple shear flow, the Reynolds number is defined as $Re = \frac{\rho\dot{\gamma}L^2}{\mu}$, $\dot{\gamma}$ being the shear rate. Subramanian & Koch (2006) analysed the effects of inertia on the motion of a nearly spherical particle in a simple shear flow. The authors have shown that the axis of symmetry of a neutrally buoyant slightly prolate spheroid migrates toward the direction of vorticity, while that of an slightly oblate spheroid drifts toward the shearing plane. It is seen from the above results that while the axis of symmetry of a fiber drifts towards the shearing plane, that of a nearly spherical prolate spheroid drifts towards the vorticity vector of the ambient shear flow. This indicates the presence of a bifurcation in orientation dynamics occurring at a critical particle aspect ratio. No literature has, however, been found on the effects of inertia and viscoelasticity on a spheroidal particle (prolate or oblate) of an arbitrary aspect ratio spheroidal particle placed in a simple shear flow. Our analysis, being applicable for an arbitrary aspect ratio spheroidal particle, will allow one to calculate this critical aspect ratio.

## 1.2 Motivation and Objectives

As a first step in understanding suspensions of anisotropic particles, we have investigated the free fall orientation of spheroidal particles in a quiescent fluid and the orientation dynamics of spheroidal particles in simple shear flow as a function of the aspect ratio. The orientation dynamics of a spheroidal particle is thus taken to be representative of that of a general axisymmetric particle. The knowledge of the motion of a single particle in a flow can be directly applied to the analysis of a dilute sedimenting suspension and the rheology of a dilute suspension of neutrally buoyant particles. By dilute, we mean the limit $\phi << 1$, where $\phi$ is the hydrodynamic volume fraction. The hydrodynamic volume fraction ($\phi$) is defined as the ratio of the volume occupied by the spheres circumscribing the spheroidal particles to the total volume occupied by the suspension. Each particle in a dilute suspension is effectively isolated since interparticle hydrodynamic interactions are negligible.

The rheological properties and the average sedimentation velocity depend on the probability distribution of orientations among all the suspension particles. We have analysed the role of inertia and viscoelasticity both of which are expected to lead to

1) a unique terminal orientation of a sedimenting spheroidal particle

2) the existence of a unique preferred orbit for a neutrally buoyant spheroidal particle in simple shear flow,

and hence enable us in calculating the rheological properties of a suspensions of these particles independent of their initial orientation distribution. We assume in our analysis that the Peclet number(Pe), which is defined as the ratio of the Brownian diffusion time scale ($\frac{L^2}{D}$, where D is the Brownian diffusivity) to the externally

imposed flow time scale ($\frac{L}{U}$ for sedimentation and $\dot{\gamma}^{-1}$ for simple shear flow), to be very large. Thermal effects may be neglected when considering the dynamics of particles larger than $10\mu$. The ratio of the Reynolds to the Peclet number ($Re/Pe$) is a characteristic of the system and is independent of the externally imposed flow. So, as $Re$ increases, $Pe$ also increases, making the system increasingly athermal. Our analysis assumes $Pe \to \infty$ and $\phi \to 0$, and hence, the effects of factors such as Brownian motion, hydrodynamic interactions, etc. on the particle orientation have been neglected.

In this thesis, we aim to determine the torque on a non-Brownian spheroidal particle sedimenting in a quiescent viscoelastic fluid as a function of its initial orientation, and to determine if, for a neutrally buoyant non-Brownian spheroidal particle, rotating in a simple shear flow, there exists a unique stable orbit among the single-parameter family of periodic orbits (Jeffery orbits) known to exist in the inertialess limit. Both the sedimentation and the shear flow problems have a degenerate character in the inertialess Newtonian limit, and one expects inertia and viscoelasticity to remove this degeneracy. As is evident from the discussion in the earlier sections, each of these problems have a long history of both theoretical and experimental work. The novel aspect of our work lies in the method of approach. We use the formalism of vector spheroidal harmonics developed by Kushch (Kushch & Sangani (2003)). The method is a generalisation of the well-known spherical harmonics formulation for Stokes flow problem (Kim & Karrila (1991)), and therefore lends itself naturally to the analysis of spheroids of an arbitrary aspect ratio.

## 1.3 Thesis layout

The thesis is structured as follows. The problem formulation has been presented in the second chapter. In particular, this chapter involves a formulation for solving the Stokes equations in spheroidal coordinates (both prolate and oblate) and, use of the generalised reciprocal theorem with these solutions to determine the effects of inertia and viscoelasticity in sedimentation and simple shear flow. The third chapter is devoted to the determination of the required Stokes velocity disturbance fields using Kushch's spheroidal harmonics formulation (Kushch & Sangani (2003)), and the results for the sedimentation and simple shear flow problems. In the final chapter,we comment on possible extensions of the present work that can be carried out in the future.

CHAPTER 2

# KUSHCH'S FORMULATION AND LORENTZ RECIPROCAL THEOREM : PROBLEM FORMULATION

## Introduction

Kushch's formulation for vector spheroidal harmonics (Kushch & Sangani (2003)) and the generalised reciprocal theorem (Happel & Brenner (1973), Leal (1980), Subramanian & Koch (2005), Subramanian & Koch (2006)) have been used to find:

(1) the inertial and viscoelastic torques on a sedimenting spheroid in a quiescent viscoelastic (second-order) fluid, and

(2) the effect of inertia and viscoelasticity on the angular velocity of a neutrally buoyant torque-free spheroid rotating in simple shear flow of a second-order fluid.

In this chapter we introduce Kushch's formulation and the generalised reciprocal theorem and apply it to the aforementioned problems.

## 2.1 Kushch's Formulation

A novel analytical framework constructed by Kushch and his co-workers (Kushch & Sangani (2003)) is applied here to solve a series of problems for a viscous fluid with suspended spheroidal particles. The basic idea of the method is the multi pole

expansion, a method that has been applied to determine the interactions among N spherical particles [see Sangani & Mo (1996)] when the motion of the fluid is governed by the Stokes equations. The structure of the spheroidal harmonics formalism developed by Kushch is analogous to the well-known solution in terms of spherical harmonics that is in standard use [see Chapter-4 of Kim & Karrila (1991)]. Kushch earlier had developed a similar formalism to solve the Lame's equations (the equations of linear elasticity) in a spheroidal basis to find the microstresses and effective elastic moduli of a solid reinforced by periodically distributed spheroidal particles [see Kushch (1997)]. The new features added by Kushch & Sangani (2003) are the vectorial partial solutions of the Stokes equations in the spheroidal coordinate system and the re-expansion formulae due to the position change of the reference coordinate system. The implementation of the spheroidal harmonics formulation reduces the boundary-value problem in a multi-particle system to a set of linear algebraic equations by exact satisfaction of the boundary conditions at all the interfaces. In practice the system of equations is truncated at a certain order, which is equivalent to the neglect of multipoles higher than that order. This formulation allows for an analytical description of the flow around spheroidal particles (either prolate or oblate spheroids) of an arbitrary aspect ratio. Hence, one can vary the aspect ratio of a prolate spheroid and reach an infinitely slender fiber at one end of the spectrum and reach a near-sphere at the other end [see figure 2.1]. Similarly, by varying the aspect ratio of the oblate spheroid, one can reach a flat disk at one end and a near sphere at the other end [see figure 2.2]. Thus, this formulation allows one to conduct a detailed study of the effect of particle aspect ratio on the bulk properties of suspensions. Kushch and his co-workers (Kushch & Sangani (2003)) developed this technique to solve the N-particle interaction problem in the Stokes limit for a specified micro-structure. We will be extending the formalism

to study the effects of tiny departures, due to inertia or viscoelasticity, from the Stokes scenario on the orientation dynamics of a single particle.

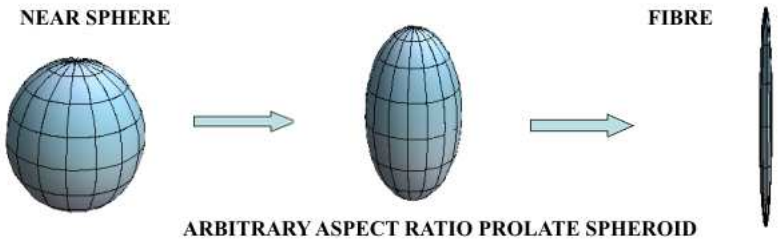


Figure 2.1: Range of particle shapes that can be studied by varying the aspect ratio of a prolate spheroid

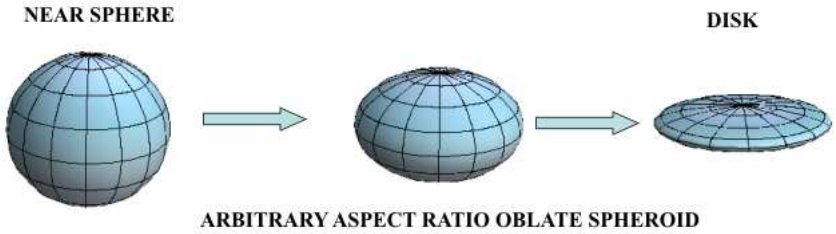


Figure 2.2: Range of particle shapes that can be studied by varying the aspect ratio of an oblate spheroid

### 2.1.1 Prolate and oblate spheroidal coordinate systems

The most convenient form of the solutions to the Stokes equations for the problems of interest is that corresponding to a spheroidal coordinate system. This is, of course, because the bounding surface of the spheroidal particle now reduces to a constant coordinate surface.

In the prolate spheroidal coordinate system, $(\xi, \eta, \phi)$ are the three independent coordinates. $\xi, \eta$, and $\phi$ are related to the Cartesian coordinates(x,y,z) by:

$$x + iy = d\sqrt{\xi^2 - 1}\sqrt{1 - \eta^2}\exp(i\phi), z = d\xi\eta; \tag{2.1}$$

$$1 \leq \xi \leq \infty, |\eta| \leq 1, 0 \leq \phi < 2\pi$$

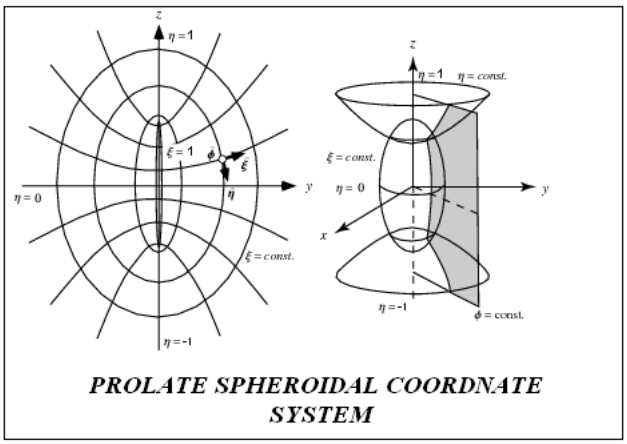


Figure 2.3: The constant coordinate surfaces in a prolate spheroidal coordinate system

Figure 2.3 shows the topology of the constant coordinate surfaces in a prolate spheroidal coordinate system. By assigning a series of different values to $\xi$, one generates a family of confocal prolate spheroids with inter-foci distance being equal to 2d. Constant $\eta$ surfaces represent a family confocal two-sheeted hyperboloids. The third set of coordinates $\phi$ consists of planes passing through the axis of symmetry, the z axis.

Let $\xi_0$ represent the surface of the particle and $\xi > \xi_0$ represent the domain outside the particle. With increasing $\xi$, the constant $\xi$ spheroids approach a spherical shape, and correspondingly, the constant $\eta$ surfaces approach a conical geometry, the latter being the second family of constant coordinate surfaces in a spherical coordinate system. Constant $\phi$ surfaces are planes that pass through the axis of

symmetry (the z axis), and $\phi$ is usually referred to as the azimuthal angle. This also shows that in order to proceed to the limiting case of spherical coordinates, the relevant limit is that of $\xi \to \infty$ and $d \to 0$ with $(d\xi)$ fixed. The quantity $(d\xi = r)$ represents the radius of the limiting spherical surface. On the other hand, for $\xi$ approaching unity, the prolate spheroids become increasingly slender, tending to an infinitely slender fiber at $\xi = 1$.

Similarly, one may now define the oblate spheroidal coordinate system. The oblate spheroidal coordinate system may be obtained by replacing $\xi$ by $i\sqrt{\xi^2 - 1}$ and $d$ by $-id$ in the expressions for the prolate spheroidal coordinate system given above [see equation (2.1)].

Again denoting $(\xi, \eta, \phi)$ as the three independent coordinates, $\xi, \eta$, and $\phi$ are related to the Cartesian coordinates (x,y,z) by:

$$x + iy = d\xi\sqrt{1 - \eta^2}\exp(i\phi), z = d\sqrt{\xi^2 - 1}\eta; \tag{2.2}$$

$$1 \leq \xi \leq \infty, |\eta| \leq 1, 0 \leq \phi < 2\pi$$

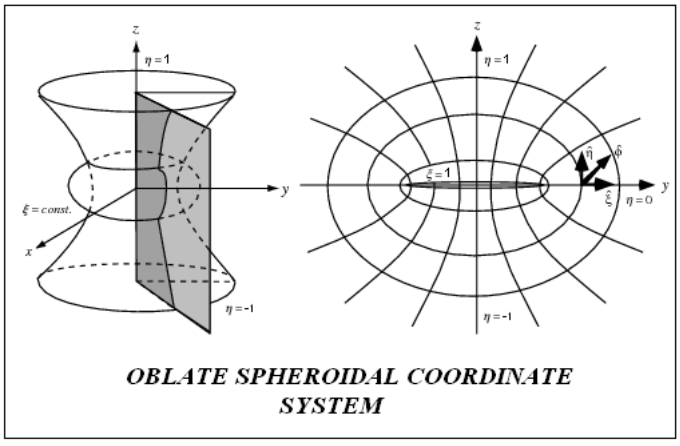


Figure 2.4: The constant coordinate surfaces in an oblate spheroidal coordinate system

Figure 2.4 shows the topology of the constant coordinate surfaces in an oblate spheroidal coordinate system. By assigning a series of different values to $\xi$, one generates a family of confocal oblate spheroids with inter-foci distance being equal to 2d. Constant $\eta$ surfaces represent a family confocal single-sheeted hyperboloids. The third set of constant coordinates $\phi$ surfaces consists of planes passing through the axis of symmetry, and is thus the same as the azimuthal coordinate in a spherical coordinate system. In a manner similar to the prolate coordinate system, the limit $\xi \to \infty$ and $d \to 0$ with $(d\xi)$ fixed leads to a spherical coordinate system. The quantity $(d\xi = r)$ represents the radius of the limiting spherical surface. On the other hand, for $\xi$ approaching unity, the oblate spheroids become increasingly flat, tending to an infinitely thin disc at $\xi = 1$.

*(see Appendix A for further details on the prolate and oblate coordinate systems)*

### 2.1.2 Partial vectorial solutions of the Stokes equations in spheroidal coordinates

Here we discuss the set of decaying partial vectorial solutions of Stokes equation as introduced by Kushch and his co-workers (Kushch & Sangani (2003)). Any exterior velocity field may be expressed as a linear combination of these decaying solutions. We only deal with exterior problems since the spheroidal particle, both in sedimentation and simple shear flow, is in an unbounded fluid domain.

The decaying vectorial solutions in the prolate spheroidal coordinate system are given by:

$$
\begin{aligned}
\mathbf{S}_{ts}^{(1)} &= \mathbf{e}_1 F_{t+1}^{s-1} - \mathbf{e}_2 F_{t+1}^{s+1} + \mathbf{e}_3 F_{t+1}^{s}; \qquad (2.3)\\
\mathbf{S}_{ts}^{(2)} &= \frac{1}{t}\left[\mathbf{e}_1(t+s)F_t^{s-1} + \mathbf{e}_2(t-s)F_t^{s+1} + \mathbf{e}_3 s F_t^s\right];\\
\mathbf{S}_{ts}^{(3)} &= \mathbf{e}_1\left\{-(x-iy)\mathrm{D}_2 F_{t-1}^{s-1} - \left[(\xi_0)^2-1\right] d\mathrm{D}_1 F_t^s + (t+s-1)(t+s)\beta_{-(t+1)}F_{t-1}^{s-1}\right\}\\
&\quad +\mathbf{e}_2\left\{(x+iy)\mathrm{D}_1 F_{t-1}^{s+1} - \left[(\xi_0)^2-1\right] d\mathrm{D}_2 F_t^s - (t-s-1)(t-s)\beta_{-(t+1)}F_{t-1}^{s+1}\right\}\\
&\quad +\mathbf{e}_3\left[z\mathrm{D}_3 F_{t-1}^s - (\xi_0)^2 d\mathrm{D}_3 F_t^s - C_{-(t+1),s}F_{t-1}^s\right];
\end{aligned}
$$

where $\beta_t = \frac{t+3}{(t+1)(2t+3)}$; further,

$C_{ts} = (t+s+1)(t-s+1)\beta_t;\ \ t = 0, 1, ...;\ \ |s| \le t.$

$\mathbf{e}_1 = (\mathbf{e}_x + i\mathbf{e}_y)/2,\ \mathbf{e}_2 = (\mathbf{e}_x - i\mathbf{e}_y)/2,\ \mathbf{e}_3 = \mathbf{e}_z,$

$D_1 = (\partial/\partial x - i\partial/\partial y),\ \ D_2 = (\partial/\partial x + i\partial/\partial y),\ \ D_3 = (\partial/\partial z).$

The z-axis of the Cartesian coordinate system is the axis of symmetry of the spheroidal coordinate system.

The functions $F_t^s = F_t^s(\mathbf{r}, d)$ are solid spheroidal harmonics of the form $F_t^s = Q_t^s(\xi)Y_t^s(\eta,\phi)$. $Y_t^s(\eta,\phi) = P_t^s(\eta)\exp(is\phi)$ are the scalar surface harmonics and $P_t^s(\eta)$ and $Q_t^s(\xi)$ are the associated Legendre polynomials of the first and second kind, respectively [Morse & Feshbach (1953)]. The functions $Q_t^s(\xi) \to 0$ as $\xi \to \infty$, and this provides the decaying nature of the velocity field for an exterior problem. Thus, the index "t" indicates the rapidity of decay of the disturbance velocity field. The index "s" governs the variation of the velocity field with the azimuthal angle. Thus, s=0 for an axisymmetric disturbance velocity field.

The expressions for the first few Legendre polynomials of the first kind are given

below:

$$
\begin{aligned}
P_0^0 &= 1, \\
P_1^0 &= \eta, \\
P_1^1 &= \sqrt{1-\eta^2}, \\
P_2^1 &= 3\eta\sqrt{1-\eta^2}, \\
P_2^2 &= 3(1-\eta^2).
\end{aligned}
$$

The expressions for the first few Legendre polynomials of the second kind are given below:

$$
\begin{aligned}
Q_0^0 &= \frac{1}{2}\log\left(\frac{\xi+1}{\xi-1}\right), \\
Q_1^0 &= \frac{\xi}{2}\log\left(\frac{\xi+1}{\xi-1}\right) - 1, \\
Q_1^1 &= \frac{1}{4}\left(3\xi^2-1\right)\log\left(\frac{\xi+1}{\xi-1}\right) - \frac{3}{2}\xi, \\
Q_2^1 &= \frac{1}{2}\sqrt{(\xi^2-1)}\log\left(\frac{\xi+1}{\xi-1}\right) - \frac{\xi}{\sqrt{\xi^2-1}}, \\
Q_2^2 &= \frac{3}{2}\left(\xi^2-1\right)\log\left(\frac{\xi+1}{\xi-1}\right) - \left(\frac{3\xi^2-5\xi}{\xi^2-1}\right).
\end{aligned}
$$

A few properties of these functions $\boldsymbol{S}_{ts}^{(i)}$'s are:

$\boldsymbol{\nabla}.\boldsymbol{S}_{ts}^{(i)} = 0,\ i = 1, 2, 3,$

$\boldsymbol{\nabla} \times \boldsymbol{S}_{ts}^{1} = 0,\ d\boldsymbol{\nabla} \times \boldsymbol{S}_{ts}^{(2)} = -i\boldsymbol{\nabla} \times \widetilde{\boldsymbol{S}}_{ts}^{(1)},\ d\boldsymbol{\nabla} \times \boldsymbol{S}_{ts}^{(3)} = -2i\boldsymbol{\nabla} \times \widetilde{\boldsymbol{S}}_{ts}^{(2)},$

where $\widetilde{\boldsymbol{S}}_{ts}^{(1)}$ and $\widetilde{\boldsymbol{S}}_{ts}^{(2)}$ have the form of equation (2.3), with $F_t^s$ replaced by $dD_3F_{t-1}^s$. The Cartesian derivatives of the solid spheroidal harmonics are related by

$D_3F_{t-1}^s = D_1F_{t-1}^{s+1} = -D_2F_{t-1}^{s-1}$.

Further, $\boldsymbol{\nabla}^2\boldsymbol{S}_{ts}^{(i)} = 0, (i = 1, 2)$ implying that these are vectorial harmonic functions and therefore do not have any disturbance pressure field associated with them in the Stokes limit. Since $\boldsymbol{\nabla} \times \boldsymbol{S}_{ts}^{(1)} = 0$, $\boldsymbol{S}_{ts}^{(1)}$ must be the gradient of a scalar and hence will give rise to potential flow field. On the other hand, $\boldsymbol{S}_{ts}^{(3)}$ is a biharmonic function ($\boldsymbol{\nabla}^4\boldsymbol{S}_{ts}^{(3)}$=0), and gives rise to a non-trivial disturbance pressure field. Since $\nabla^2\boldsymbol{S}_{ts}^{(3)} = \frac{2}{d}\boldsymbol{\nabla}D_t^s$ ($D_t^s = dD_3F_{t-1}^s$), this identity helps in finding out the pressure field corresponding to the velocity field obtained using the series of partial solutions.

The similarity in the structure of vectorial solutions of Stokes equations in the spheroidal and spherical coordinate systems is illustrated in *Appendix C*.

Now, we proceed to discuss the underlying idea of this method. A body-fixed Cartesian coordinate system is chosen with the origin placed at the spheroid's center of mass and with z-axis as the axis of symmetry of the particle. To describe the spheroidal particles conveniently we will use the spheroidal coordinates$(\xi, \eta, \phi)$, which are related to the Cartesian coordinates via equations (2.1) and (2.2). In the notation of the spheroidal coordinate systems introduced earlier, the surface of the spheroidal particle is denoted by $\xi = \xi_0$. The motion of the incompressible viscous fluid is governed by the Stokes equations in the exterior domain $\xi > \xi_0$. The Stokes equations and the mass conservation equation for an incompressible fluid are given by:

$$\mu\nabla^2\mathbf{u} = \nabla p; \quad \nabla \cdot \mathbf{u} = 0; \tag{2.4}$$

where $\mathbf{u}$ is the velocity field, p is the pressure field and $\mu$ is the viscosity of the fluid. The no-slip boundary condition at the particle surface can be written as:

$$\mathbf{u}\,|_{\xi=\xi_0} = \mathbf{U} + \mathbf{r}_0 \times \mathbf{\Omega}, \quad \mathbf{r}_0 = \mathbf{x} - \mathbf{x}_0; \tag{2.5}$$

where $\mathbf{U}$ is the translational velocity of the particle, $\mathbf{x}_0$ is the position vector of the center of the particle, $\mathbf{x}$ is a vector that lies on the surface of the particle, and $\mathbf{\Omega}$ denotes the particle's angular velocity. Also, as one goes far away from the particle surface the disturbance velocity decays to zero and the total velocity equals the externally imposed velocity $\boldsymbol{U}^{\infty}$. Thus,

$$\mathbf{u} \to \boldsymbol{U}^{\infty} \text{ as } \|\mathbf{r}\| \to \infty. \tag{2.6}$$

It follows from the last condition that the series of multipole expansion of the induced disturbance velocity field will contain only decaying singular partial solutions $\mathbf{S}_{ts}^{(i)}$ which were introduced earlier[see equations (2.3)]: Thus,

$$\mathbf{u} = \sum_{i=1}^{3} \sum_{t=0}^{\infty} \sum_{s=-t}^{t} A_{ts}^{(i)} \mathbf{S}_{ts}^{(i)} \left(\mathbf{r},\ d\right), \tag{2.7}$$

where the $\mathbf{A}_{ts}^{(i)}$ are the multipole strengths to be found from the boundary conditions in equation (2.5). One obtains,

$$\mathbf{U} + \mathbf{r}_0 \times \mathbf{\Omega} = \sum_{i=1}^{3} \sum_{t=0}^{\infty} \sum_{s=-t}^{t} A_{ts}^{(i)} \mathbf{S}_{ts}^{(i)}|_{\xi=\xi_0}. \tag{2.8}$$

The three decaying partial vectorial solutions of the Stokes equation (2.3) evaluated at $\xi = \xi_0$ in the prolate spheroidal coordinate system are given below [see Kushch & Sangani (2003)]:

$$
\begin{aligned}
\mathbf{S}_{ts}^{(1)}\,|_{\xi=\xi_0} &= \mathbf{e}_1 Q_{t+1}^{s-1} Y_{t+1}^{s-1} - \mathbf{e}_2 Q_{t+1}^{s+1} Y_{t+1}^{s+1} + \mathbf{e}_3 Q_{t+1}^{s} Y_{t+1}^{s}; \qquad (2.9)\\
\mathbf{S}_{ts}^{(2)}\,|_{\xi=\xi_0} &= \mathbf{e}_1 \frac{(t+s)}{t} Q_t^{s-1} Y_t^{s-1} + \mathbf{e}_2 \frac{(t-s)}{t} Q_t^{s+1} Y_t^{s+1} + \mathbf{e}_3 \frac{s}{t} Q_t^{s} Y_t^{s};\\
\mathbf{S}_{ts}^{(3)}\,|_{\xi=\xi_0} &= \mathbf{e}_1 \left\{ -(t-s+1)\xi_0 Q_t^{s-1} + (t+s-1)\left[1+(t+s)\beta_{-(t+1)}\right] Q_{t-1}^{s-1} \right\} Y_{t-1}^{s-1}\\
&\quad + \mathbf{e}_2 \left\{ (t-s-1)\xi_0 Q_t^{s+1} - (t-s-1)\left[1+(t-s)\beta_{-(t+1)}\right] Q_{t-1}^{s+1} \right\} Y_{t-1}^{s+1}\\
&\quad + \mathbf{e}_3 \left\{ -(t-s)\xi_0 Q_t^{s} - C_{-(t+1),s} Q_{t-1}^{s} \right\} Y_{t-1}^{s},
\end{aligned}
$$

where $Q_t^s = Q_t^s(\xi_0)$ and $Y_t^s = \frac{(t-s)!}{(t+s)!} P_t^s(\eta)\exp(is\varphi)$ are the scalar surface harmonics. These partial vectorial solutions evaluated at the surface of the particle will help us solve the system of simultaneous linear equations [see (2.8)] to find the unknown mutipole coefficients $A_{ts}^{(i)}$.

One may proceed similarly for the oblate coordinate system. The partial vectorial decaying solutions in the oblate coordinate system may be obtained from the above expressions, valid for prolate spheroidal coordinates by replacing $\xi$ by $i\sqrt{\xi^2-1}$ and $d$ by $-id$. Thus the decaying partial vectorial solutions of the Stokes equations in an oblate coordinate system are given by:

$$
\begin{aligned}
\mathbf{S}_{ts}^{(1)} &= \mathbf{e}_1 F_{t+1}^{s-1} - \mathbf{e}_2 F_{t+1}^{s+1} + \mathbf{e}_3 F_{t+1}^{s}; \qquad (2.10)\\
\mathbf{S}_{ts}^{(2)} &= \frac{1}{t}\left[ \mathbf{e}_1 (t+s) F_t^{s-1} + \mathbf{e}_2 (t-s) F_t^{s+1} + \mathbf{e}_3 s F_t^{s} \right];\\
\mathbf{S}_{ts}^{(3)} &= \mathbf{e}_1 \left\{ -(x-iy)\mathrm{D}_2 F_{t-1}^{s-1} - i\left[(\xi_0)^2\right] d\mathrm{D}_1 F_t^s + (t+s-1)(t+s)\beta_{-(t+1)} F_{t-1}^{s-1} \right\}\\
&\quad + \mathbf{e}_2 \left\{ (x+iy)\mathrm{D}_1 F_{t-1}^{s+1} - i\left[(\xi_0)^2\right] d\mathrm{D}_2 F_t^s - (t-s-1)(t-s)\beta_{-(t+1)} F_{t-1}^{s+1} \right\}\\
&\quad + \mathbf{e}_3 \left[ z\mathrm{D}_3 F_{t-1}^{s} - i\left[(\xi_0)-1\right]^2 d\mathrm{D}_3 F_t^s - C_{-(t+1),s} F_{t-1}^{s} \right].
\end{aligned}
$$

The three decaying partial vectorial solutions of the Stokes equations (2.10) eval-

uated at $\xi = \xi_0$ in the oblate spheroidal coordinate system, are as given below:

$$
\begin{aligned}
\mathbf{S}_{ts}^{(1)}\,|_{\xi=\xi_0} &= \mathbf{e}_1 Q_{t+1}^{s-1} Y_{t+1}^{s-1} - \mathbf{e}_2 Q_{t+1}^{s+1} Y_{t+1}^{s+1} + \mathbf{e}_3 Q_{t+1}^{s} Y_{t+1}^{s}; \qquad (2.11)\\
\mathbf{S}_{ts}^{(2)}\,|_{\xi=\xi_0} &= \mathbf{e}_1 \frac{(t+s)}{t} Q_t^{s-1} Y_t^{s-1} + \mathbf{e}_2 \frac{(t-s)}{t} Q_t^{s+1} Y_t^{s+1} + \mathbf{e}_3 \frac{s}{t} Q_t^{s} Y_t^{s};\\
\mathbf{S}_{ts}^{(3)}\,|_{\xi=\xi_0} &= \mathbf{e}_1 \left\{ -(t-s+1)\left[ i\sqrt{{\xi_0}^2 - 1} \right] Q_t^{s-1} + (t+s-1)\left[ 1 + (t+s)\beta_{-(t+1)} \right] Q_{t-1}^{s-1} \right\} Y_{t-1}^{s-1}\\
&\quad + \mathbf{e}_2 \left\{ (t-s-1)\left[ i\sqrt{{\xi_0}^2 - 1} \right] Q_t^{s+1} - (t-s-1)\left[ 1 + (t-s)\beta_{-(t+1)} \right] Q_{t-1}^{s+1} \right\} Y_{t-1}^{s+1}\\
&\quad + \mathbf{e}_3 \left\{ -(t-s)\left[ i\sqrt{{\xi_0}^2 - 1} \right] Q_t^{s} - C_{-(t+1),s} Q_{t-1}^{s} \right\} Y_{t-1}^{s},
\end{aligned}
$$

where $\beta_t = \frac{t+3}{(t+1)(2t+3)}$;

$C_{ts} = (t+s+1)(t-s+1)\beta_t;\ \ t = 0, 1, ...;\ \ |s| \leq t.$

$\mathbf{e}_1 = (\mathbf{e}_x + i\mathbf{e}_y)/2,\ \mathbf{e}_2 = (\mathbf{e}_x - i\mathbf{e}_y)/2,\ \mathbf{e}_3 = \mathbf{e}_z$

These forms may then be used in the boundary conditions to again obtain a system of simultaneous linear equations to be solved for the multipole coefficients.

### 2.1.3 Force and torque calculation

The force on the particle in the prolate and oblate spheroidal coordinate systems are given by:

$$\mathbf{F} = 16\pi\mu d \left( -A_{11}^{(3)}\mathbf{e}_1 + A_{1,-1}^{(3)}\mathbf{e}_2 + \frac{1}{2}A_{10}^{(3)}\mathbf{e}_3 \right), \qquad (2.12)$$

$$\mathbf{F} = -16\pi\mu i d \left( -A_{11}^{(3)}\mathbf{e}_1 + A_{1,-1}^{(3)}\mathbf{e}_2 + \frac{1}{2}A_{10}^{(3)}\mathbf{e}_3 \right), \qquad (2.13)$$

respectively. In the above expressions $A_{ts}^{(i)}$ are the multipole strengths chosen from the boundary conditions relevant to the particular problem. Similarly, the expres-

sions for the torque on the prolate and oblate spheroids, respectively, are:

$$\mathbf{M} = \frac{16}{3}\pi\mu i d^2 \left( -A_{11}^{(3)}\mathbf{e}_1 + A_{1,-1}^{(3)}\mathbf{e}_2 - \frac{1}{2}A_{10}^{(3)}\mathbf{e}_3 \right) \tag{2.14}$$

$$\mathbf{M} = -\frac{16}{3}\pi\mu i d^2 \left( -A_{11}^{(3)}\mathbf{e}_1 + A_{1,-1}^{(3)}\mathbf{e}_2 - \frac{1}{2}A_{10}^{(3)}\mathbf{e}_3 \right) \tag{2.15}$$

## 2.2 Generalised reciprocal theorem

The generalised reciprocal theorem relates the velocity and stress fields of two problems, the actual problem $(\boldsymbol{\sigma}^{(1)}, \boldsymbol{u}^{(1)})$ and a test problem $(\boldsymbol{\sigma}^{(2)}, \boldsymbol{u}^{(2)})$ for which the solution is known. Both $(\boldsymbol{\sigma}^{(1)}, \boldsymbol{u}^{(1)})$ and $(\boldsymbol{\sigma}^{(2)}, \boldsymbol{u}^{(2)})$ are solutions of the flow past the same body but with different boundary conditions and possibly governed by different dynamical equations.

In our case, the actual problem is that of a spheroidal particle undergoing a specified motion in a non-Newtonian fluid. The non-Newtonian fluid used in the experiments (described in Chapter-1) is a dilute polymer solution at reasonably small shear rates. At these small shear rates, the effects of viscoelasticity are small, and the fluid may be modelled as a second-order fluid. In other words, the fluid is slightly non-Newtonian , and the Deborah number $De = \frac{\lambda}{t_{flow}}$ is much smaller than unity. Here, $t_{flow}$ is the externally imposed flow time scale and $\lambda$ is the intrinsic relaxation time of the non-Newtonian fluid. The Deborah number is the key dimensionless parameter in non-Newtonian fluids, and is a measure of the degree of viscoelasticity. If the Deborah number is small, then thermal motions keep the polymer molecules more or less in their equilibrium configurations, and the polymeric fluid shows only a minor qualitative difference from a Newtonian fluid. Thus, Newtonian behavior is obtained in the limit $De = 0$. When the Deborah

number is large, polymer molecules distorted by the flow will not have time to relax during the time scale of the experiment. In the limit $De \rightarrow \infty$ the flow time scale is so small that the polymer molecules have no time to relax in response to changes in configuration imposed by the flow. In this limit, the elastic component of the response is important.

In the limit of slow, slowly varying flows, the fluid rheology is governed by the retarded motion expansion [see Bird *et al.* (1987) and Larson (1988)]. To $O(De)$, the retarded motion expansion reduces to the second-order fluid constitutive equation. Thus, the second-order fluid rigorously accounts for the first effects of viscoelasticity in slow flows. The second-order fluid constitutive equation predicts a constant viscosity and constant normal stress differences in a simple shear flow, but fails to capture the variation of the viscosity and normal stress coefficients.

The appropriate non-dimensional equation of motion for the problem of interest is as given below:

$$Re\left(\frac{D\mathbf{u}^{(1)}}{Dt}\right) = \nabla \cdot \boldsymbol{\sigma}^{(1)}; \tag{2.16}$$

$$\nabla.\mathbf{u}^{(1)} = 0 \tag{2.17}$$

In equation (2.16), $\boldsymbol{\sigma}^{(1)}$ is the total stress tensor of the non-Newtonian fluid, and $\mathbf{u}^{(1)}$ is the disturbance velocity field of the actual problem; $\left(\frac{D\mathbf{u}^{(1)}}{Dt}\right)$ is the convective acceleration. The scales chosen for non-dimensionalization of the above equation are as follows. The length scale is the major diameter of the spheroid ($L$=$d\xi_0$). Taking the major axis of the spheroid as the relevant scale ensures that one obtains the correct length scale even in the limit of a slender body; slender body theory says that it is the length and not the diameter of the body that is the correct length scale characterizing the variation of the disturbance velocity field in the limit of large aspect ratio. An appropriate velocity scale $U$ is chosen. The

stress $\boldsymbol{\sigma}$ for viscous flows scales as $\frac{\mu U}{L}$. The Reynolds number, the ratio of inertial to viscous forces, is based on the major diameter of the spheroid, and is given by $Re = \frac{\rho U L}{\mu}$. $Re = 0$ indicates that there is a instantaneous balance between the pressure and viscous forces every where in the fluid and the fluid motion is in the Stokes regime. As the Reynolds number is increased, inertia of the fluid becomes important.

The total stress in the actual problem is the stress in a second-order fluid, and is composed of two parts, the Newtonian stress $\boldsymbol{\sigma}_N^{(1)}$, linear in the velocity gradient tensor and the non-Newtonian stress $\boldsymbol{\sigma}_{NN}^{(1)}$ which is a non-linear function of the velocity gradient tensor. Thus,

$$\boldsymbol{\sigma}^{(1)} = \boldsymbol{\sigma}_N^{(1)} + De\left(\boldsymbol{\sigma}_{NN}^{(1)}\right) \tag{2.18}$$

where $De$ is the Deborah number defined earlier. The non-dimensional Newtonian stress can be written as:

$$\boldsymbol{\sigma}_N^{(1)} = -p^{(1)}\boldsymbol{I} + 2\boldsymbol{E}^{(1)}, \tag{2.19}$$

where $p^{(1)}$ is the pressure field and $\boldsymbol{E}^{(1)} = \frac{1}{2}(\nabla \boldsymbol{u}^{(1)} + \nabla \boldsymbol{u}^{(1)^t})$ is the strain rate tensor of the actual problem. The non-dimensional non-Newtonian stress can be written as the sum of a co-rotational ($\boldsymbol{\sigma}_{NNC}^{(1)}$) and a quadratic ($\boldsymbol{\sigma}_{NNQ}^{(1)}$) contribution :

$$\boldsymbol{\sigma}_{NN}^{(1)} = \left(\boldsymbol{\sigma}_{NNC}^{(1)} + \boldsymbol{\sigma}_{NNQ}^{(1)}\right), \tag{2.20}$$

where the co-rotational portion of the non-Newtonian stress is given by

$$\boldsymbol{\sigma}^{(1)}_{NNC} = 2\epsilon_1 \left( \frac{\partial \boldsymbol{E}^{(1)}}{\partial t} + \boldsymbol{\nabla}.\left(\boldsymbol{u}\boldsymbol{E}^{(1)}\right) + \left(\boldsymbol{W}^{(1)}.\boldsymbol{E}^{(1)}\right) + \left(\boldsymbol{W}^{(1)}.\boldsymbol{E}^{(1)}\right)^t \right),$$

and the part of the non-Newtonian stress that is quadratic in the strain rate is given by:

$$\boldsymbol{\sigma}^{(1)}_{NNQ} = 4(1+\epsilon_1)\boldsymbol{E}^{(1)}.\boldsymbol{E}^{(1)}.$$

Here, $\boldsymbol{W}^{(1)}=\frac{1}{2}(\nabla \boldsymbol{u}^{(1)} - \nabla \boldsymbol{u}^{(1)^t})$ is the vorticity tensor and $\epsilon_1$ is an intrinsic fluid property. $\epsilon_1$ is defined as $\frac{-\boldsymbol{\psi_1}}{2(\boldsymbol{\psi_1}+\boldsymbol{\psi_2})}$, where $\psi_1$ and $\psi_2$ are the normal stress coefficients and can be defined in terms of the familiar normal stress differences, $N_1$ and $N_2$ as $\psi_1=\frac{N_1}{\dot{\gamma}^2}$ and $\psi_2=\frac{N_2}{\dot{\gamma}^2}$ [see Larson (1988) & Bird *et al.* (1987)]. The ratio of $\frac{-\boldsymbol{\psi_2}}{\boldsymbol{\psi_1}}$ typically varies from 0.01 to 0.2 for a dilute polymer solution and hence $\epsilon_1$ varies from $-0.5$ to$-0.65$.

The test problem is simply the inertialess translation of a spheroidal particle in a quiescent Newtonian fluid if the dynamical quantity of interest is the force, and rotation in a quiescent fluid if the dynamical quantity of interest is the torque. The particle in the test problem has the same orientation as the one in the problem of interest. The equations of motion and continuity of the test problem are:

$$\boldsymbol{\nabla}.\boldsymbol{\sigma}^{(2)} = 0 \tag{2.21}$$

$$\boldsymbol{\nabla}.\boldsymbol{u}^{(2)} = 0$$

where,

$$\boldsymbol{\sigma}^{(2)} = -p^{(2)}\boldsymbol{I} + 2\boldsymbol{E}^{(2)}, \tag{2.22}$$

where $p^{(2)}$ is the pressure field and $\boldsymbol{E}^{(2)}=\frac{1}{2}(\nabla \boldsymbol{u}^{(2)} + \nabla \boldsymbol{u}^{(2)^t})$ is the strain rate tensor

of the test problem.

When the generalised reciprocal theorem is applied to the actual and test problems one obtains the following identity:

$$\int_S \boldsymbol{n}.\boldsymbol{u}^{(2)}.\boldsymbol{\sigma}^{(1)}dS - \int_S \boldsymbol{n}.\boldsymbol{u}^{(1)}.\boldsymbol{\sigma}^{(2)}dS = Re\int_V \frac{D\boldsymbol{u}^{(1)}}{Dt}.\boldsymbol{u}^{(2)}dV + De\int_V \boldsymbol{\sigma}^{(1)}_{NN} : \nabla \boldsymbol{u}^{(2)}dV \tag{2.23}$$

*(see Appendix B for a derivation of the above reciprocal theorem identity)*

Here, $\mathbf{n}$ is the unit normal pointing into the fluid domain $V$ bounded by the surface $S$. If the disturbance velocity decays rapidly away from the particle, the surfaces integrals at infinity may be neglected, and the bounding surface $S$ in the integrals in (2.23) becomes that of the particle ($S_p$). The unit normal on the surface of a spheroidal particle is $\widehat{\boldsymbol{e}}_\xi$, the unit vector perpendicular to the constant $\xi$ surfaces.

### 2.2.1 Generalised reciprocal theorem applied to the sedimentation of a spheroid in a quiescent second-order fluid

In this section we use the generalised reciprocal identity (2.23) to find the torque on a sedimenting spheroidal particle in a second-order fluid. The non-dimensional equations of motion (2.16) and the boundary conditions for the actual problem are: $\mathbf{u}^{(1)}|_{\xi=\xi_o} = \mathbf{U}$, where $\mathbf{U}$ is the translational velocity of the particle, and $\mathbf{u}^{(1)} \rightarrow 0$ as $\|\mathbf{x}\| \rightarrow \infty$

Since we are interested in finding the torque acting on the sedimenting particle, we choose the test problem as a spheroidal particle of the same orientation rotating about an axis (the y-axis) perpendicular to the plane containing the vectors $\mathbf{U}$ and axis of symmetry of the particle in a quiescent Newtonian fluid in the Stokes

regime. The geometry of the two problems is shown in figure 2.5. The direction of the torque in the actual problem will determine the direction of rotation of the translating spheroidal particle.

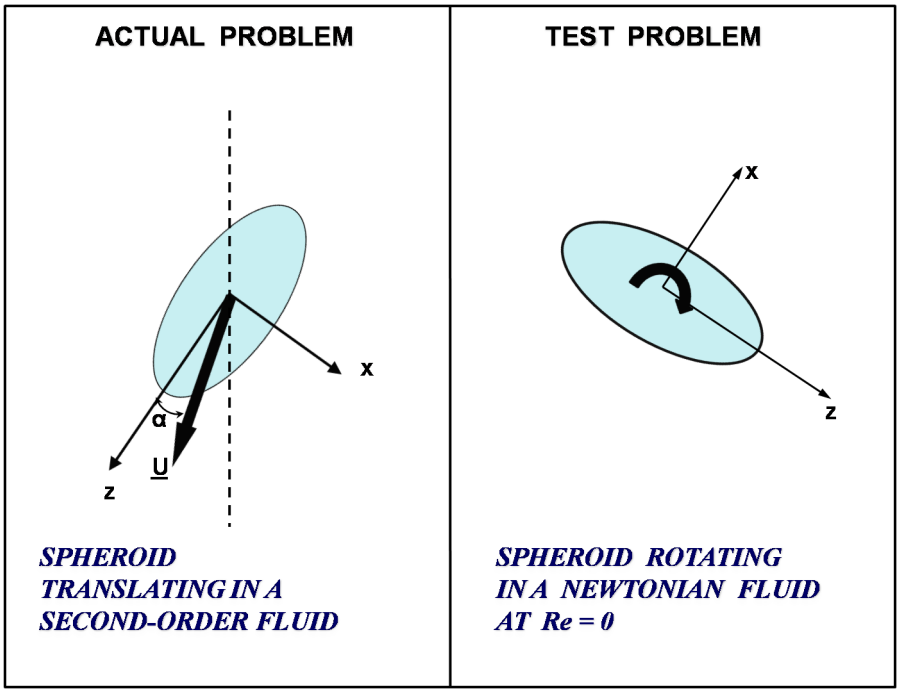


Figure 2.5: Reciprocal theorem: spheroid sedimenting in a second-order fluid

When applying the reciprocal theorem identity (2.23) to the sedimentation problem, we make use of the fact that the spheroidal particle rotating in a quiescent fluid experiences no force, but only a torque; this reduces the second surface integral (on the left hand side) in equation (2.23) to zero. In addition, the velocity of the fluid on the surface of the particle in the test problem is given by $\boldsymbol{\Omega}^{(2)} \times \boldsymbol{r_o}$, where the angular velocity $\boldsymbol{\Omega}^{(2)}$ of the test particle is a unit vector along the y-axis, and $\boldsymbol{r_o}$ represents any point on the surface of the particle. The remaining surface integral in equation (2.23) then turns out to be the torque acting on the sedimenting spheroidal particle.

With further simplification, we get the torque acting on the particle to be:

$$\boldsymbol{L}_{sed} = Re \int_V \left( \frac{D\mathbf{u}^{(1)}}{Dt} \right) \boldsymbol{.u^{(2)}} dV + De \int_V \boldsymbol{\sigma}_{NN}^{(1)} \boldsymbol{:} \nabla \boldsymbol{u}^{(2)} dV \tag{2.24}$$

where $\frac{D\mathbf{u}^{(1)}}{Dt}$ is the convective acceleration field. In lab-fixed coordinates $\frac{D\mathbf{u}^{(1)'}}{Dt} = \frac{\partial \boldsymbol{u}^{(1)'}}{\partial t} + \boldsymbol{u}^{(1)'} \boldsymbol{.\nabla u}^{(1)'}$. $\boldsymbol{u}^{(1)'}$ being the velocity field in the lab-fixed coordinates. It is more convenient, however, to use a frame of reference that translates with the particle, and the velocity field in this frame of reference is given by $\boldsymbol{u}^{(1)} = \boldsymbol{u}^{(1)'} - \boldsymbol{U}_1$, with the convective acceleration taking the form $(\boldsymbol{u}^{(1)'} - \boldsymbol{U}_1) \boldsymbol{.\nabla u}^{(1)'}$. At large distances the dominant contribution is the convection by the ambient flow $-\boldsymbol{U}_1$. The Reynolds number, $Re$, for sedimentation is defined as $\frac{\rho U L}{\mu}$, where $\rho$ is the density of the fluid, $U$ is the magnitude of the translation velocity of the spheroidal particle and ($L = d\xi_o$) is its major diameter. The Deborah number, $De$, for sedimentation is defined as $\frac{U\lambda}{L}$, where $\frac{L}{U}$ is the externally flow imposed time scale.

It can be seen from equation (2.24) that the first volume integral is the $O(Re)$ inertial torque and the second volume integral is the $O(De)$ viscoelastic torque. The two volume integrals have to be computed over the entire fluid domain $V$ to obtain the total torque acting on the particle. It turns out that the integrands decay rapidly enough for both volume integrals to be convergent over an infinite fluid domain. This convergence may be illustrated using the well- known far-field behaviour of the Stokes velocity field. In the integrand for the inertial torque the dominant contribution in $\frac{D\mathbf{u}^{(1)}}{Dt}$ comes from the term $\boldsymbol{U}_1 \boldsymbol{.} \nabla \boldsymbol{u}_1'$, linearized inertial term corresponding to convection by the ambient flow. This term decays as $O(\frac{1}{r^2})$ since the disturbance velocity due to a translating spheroidal particle, $\boldsymbol{u}_1'$, decays

as $O(\frac{1}{r})$ for large $r$; here $r$ is the distance from the spheroidal particle. The test disturbance velocity field $\boldsymbol{u}^{(2)}$ is due to a spheroidal particle rotating in a quiescent fluid decays as $O(\frac{1}{r^2})$ and $dV \sim O(r^2 dr)$. Hence, the integrand for the inertial torque is $O(\frac{1}{r^2})$ for large $r$ which is convergent, and may therefore be integrated over the entire fluid volume. The non-Newtonian stress $\boldsymbol{\sigma}^{(1)}_{NN}$ in the $O(De)$ viscoelastic torque integrand decays as $O(\frac{1}{r^4})$ for large $r$. It can then be shown that integrand in the viscoelastic torque decays as $O(\frac{1}{r^5})$, and the resultant integral over $r$ is again convergent. The convergence of the volume integral for the inertial torque indicates the regular nature of the inertial correction. This is unlike the inertial Oseen correction for the drag on a translating spheroidal particle, where the dominant contribution originates at distances of the order of the inertial screening length $(d\xi_0)Re^{-1}$.

### 2.2.2 Reciprocal theorem applied to a spheroid placed in a simple shear flow

To find the effects of inertia and viscoelasticity on a neutrally buoyant torque-free spheroid rotating in a simple shear flow, we again employ the generalised reciprocal theorem identity (2.23).

Now, we choose our test problem to be a spheroid rotating about an arbitrary axis in a quiescent Newtonian fluid in the Stokes regime; that is the same test problem as in sedimentation, since the dynamical quantity of interest is the torque in both cases. The actual problem is that of a neutrally buoyant spheroid rotating in a simple shear flow (with shear rate $\dot{\gamma}$) for small but finite inertia and weak viscoelasticity; the geometry of the two problems are shown in figure 2.6.

When applying the reciprocal theorem identity, (2.23), to the simple shear flow

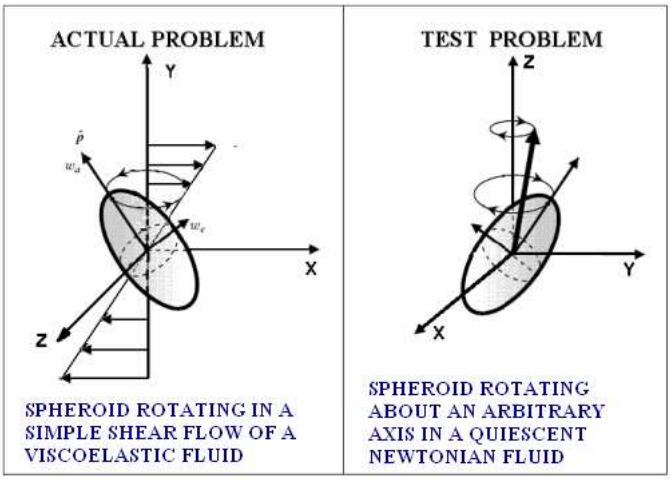


Figure 2.6: Reciprocal theorem: spheroid rotating in a simple shear flow

problem, we again make use of the fact that the test spheroid, rotating about an arbitrary axis in a quiescent fluid experiences no force, but only a torque; and that the velocity of the fluid on the surface of the test particle is given by $\boldsymbol{\Omega^{(2)}} \times \boldsymbol{r_o}$, where the angular velocity $\boldsymbol{\Omega^{(2)}}$ of the test particle is a unit vector, and $\boldsymbol{r_o}$ represents the surface of the particle. Using (2.23) we obtain the angular velocity of the spheroid in a simple shear flow, $\boldsymbol{W}_{shear}$, to be:

$$St\left(\boldsymbol{I}_{sp}.\frac{d\boldsymbol{W}_{shear}}{dt}\right).\boldsymbol{w}_2 - \boldsymbol{W_{shear}}.\boldsymbol{L}_2 = -\int_{S_p}(\boldsymbol{\Gamma}.\boldsymbol{x})\,.\left(\boldsymbol{\sigma}^{(2)}.\boldsymbol{n}\right)dS + Re\int_V \boldsymbol{f}.\boldsymbol{u}^{(2)}dV + De\int_V \boldsymbol{\sigma}^{(1)}_{NN} : \nabla\boldsymbol{u}^{(2)}dV, \tag{2.25}$$

where, $\boldsymbol{I}_{sp}$ is moment of inertia of the spheroidal particle. $\boldsymbol{L}_2$ is the torque acting on the test particle rotating in a quiescent Newtonian fluid. $\boldsymbol{f}$ is the acceleration associated with the disturbance velocity field $\boldsymbol{u}^{(1)'}$ in the actual problem, and is defined as: $\boldsymbol{f} = \frac{\partial \boldsymbol{u}^{(1)'}}{\partial \boldsymbol{t}} + \boldsymbol{\Gamma}.\boldsymbol{u}^{(1)'} + (\boldsymbol{\Gamma}.\boldsymbol{r}).\boldsymbol{\nabla}\boldsymbol{u}^{(1)'} + \boldsymbol{u}^{(1)'}.\boldsymbol{\nabla}\boldsymbol{u}^{(1)'}$.

The disturbance velocity field in simple shear flow is defined as $\boldsymbol{u}^{(1)'} = \boldsymbol{u^{(1)}} - \boldsymbol{\Gamma}.\boldsymbol{x}$, where $\boldsymbol{u}^{(1)}$ is the total velocity field in the actual problem and $\boldsymbol{\Gamma}.\boldsymbol{x}$ is the imposed shear flow. $\boldsymbol{\Gamma}$ is the transpose of the velocity gradient tensor of the ambient simple shear flow. Here, $\boldsymbol{\Gamma}$ is given as:

$$\mathbf{\Gamma} = \begin{pmatrix} 0 & 1 & 0 \\ 0 & 0 & 0 \\ 0 & 0 & 0 \end{pmatrix}$$

The boundary conditions for the disturbance velocity field are:

$\boldsymbol{u}^{(1)'} \rightarrow 0$ as $\|\mathbf{x}\| \rightarrow \infty$ and $\boldsymbol{u}^{(1)'} = (\boldsymbol{W_{shear}} \times \mathbf{x}) - \mathbf{\Gamma}.\mathbf{x}$ as $\|\boldsymbol{x}\| = \boldsymbol{x}_0$

The Reynolds number, $Re$, for a simple shear flow is defined as $\frac{\rho\dot{\gamma}L^2}{\mu}$, because the characteristic velocity scale is $\dot{\gamma}L$ and the Deborah number, $De$ is defined as $\dot{\gamma}\lambda$, where $\rho$ is the density of the fluid, $L{=}d\xi_o$ is the major diameter of the spheroid and $\dot{\gamma}$ is the shear rate. Thus, $\dot{\gamma}^{-1}$ is the externally imposed flow time scale. $St$ in (2.25) is the Stokes number and is defined as $St{=}\frac{\rho_p\dot{\gamma}L^2}{\mu}$, $\rho_p$ being the particle density. The Stokes number is a measure of particle inertia, and is usually the relevant parameter in gas-solid systems.

The first order differential equation(2.25) for the angular velocity ($\boldsymbol{W_{shear}}$) of the spheroidal particle has three contributions - the three integrals on the right hand side of equation (2.25). The first term, the surface integral, represents the Stokes solution and leads to the well known Jeffery orbit equations (Jeffery (1922)). The second and third volume integrals give the $O(Re)$ inertial correction and $O(De)$ viscoelastic correction, respectively, to the angular velocity of the neutrally buoyant spheroid placed in a simple shear flow.

In the present analysis, it is assumed that Reynolds and Deborah numbers are small but finite. As a result, the generalised reciprocal theorem allows us to calculate to a first approximation i.e. the $O(Re)$ and $O(De)$ quantities using the Stokes velocity and pressure fields in the appropriate volume integrals. The integrand of the inertial torque on a sedimenting spheroid decays as $O(\frac{1}{r^2}){\times}O(\frac{1}{r^2})dV{=}O(\frac{1}{r^2})$ for large $r$, while the integrand of the viscoelastic torque on a sedimenting spheroid

decays as $O(\frac{1}{r^4}) \times O(\frac{1}{r^3}) dV = O(\frac{1}{r^5})$ for large $r$ ($dV \sim O(r^2 dr)$), both of these are convergent, and can be integrated over the entire volume of the fluid.

———————————-

CHAPTER 3

# CANONICAL VELOCITY FIELDS AND SEDIMENTATION TORQUES : RESULTS

## Introduction

In this chapter we present the results that we have obtained using Kushch's formulation (Kushch & Sangani (2003)) and the generalised reciprocal theorem (Happel & Brenner (1973)) which have been introduced in the previous chapter. The canonical velocity fields required for the evaluation of the torque and angular velocity integrals obtained, using Kushch's formalism are presented in this chapter. The analytical results for the $O(\mathrm{Re})$ and $O(\mathrm{De})$ torques acting on the sedimenting spheroid, and the corresponding corrections to the angular velocity of a neutrally buoyant spheroid in a simple shear flow, obtained using the generalised reciprocal theorem are presented. The significance of these results are discussed herein.

## 3.1 Canonical velocity fields

This section discusses a few simple velocity fields, arising from certain canonical motions of a single spheroidal particle, which are constructed using the vectorial partial solutions of the Stokes equation in the spheroidal coordinate system [see equations(2.3)]. Further, these elementary velocity fields are used to generate the actual and test disturbance velocity fields needed in the reciprocal theorem formulation.

The velocity field induced by the motion of the spheroid reduces to the velocity field induced by a sphere in the same ambient flow in the limit $\xi_0 \to \infty$, $\xi \to \infty$, $d \to 0$ and $\eta \to \cos\theta$, such that $\xi d \to r$ and $\xi_0 d \to a$ are finite; here $r$ is the radial coordinate in the spherical coordinate system, $a$ is the particle radius and $\theta$ is the polar angle of the spherical coordinate system. The limiting forms of the various canonical velocity disturbance fields for a spheroidal particle were verified in this manner, since the expressions for the disturbance velocity fields generated by the motion of a spherical particle are well documented [see Kim & Karrila (1991)].

Some of the velocity fields were also verified by comparison with the same velocity field obtained using a different method - the singularity method of Chwang and Wu valid for Stokes flows [See T.Chwang & Wu (1974) and Chwang & Wu (1975)].

### 3.1.1 Disturbance velocity field due to a translating spheroid

Herein the disturbance velocity fields due to the translation of a spheroidal particle along the three Cartesian directions (x, y and z) are presented. The disturbance velocity field for translation in an arbitrary direction, needed in the reciprocal theorem formulation, can be found by a suitable linear combination of these three disturbance velocity fields.

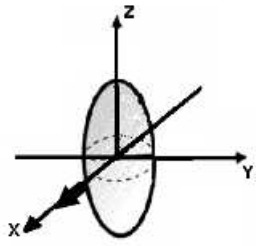


Figure 3.1: Prolate spheroid translating along X-axis

The disturbance velocity field generated due to a prolate spheroid translating along the X-axis with a velocity of magnitude U, as shown in figure 3.1, is given by

$$\mathbf{u}_x^t = A_x^t \left( \mathbf{S}_{1,1}^{(3)} - \mathbf{S}_{1,-1}^{(3)} \right). \tag{3.1}$$

The constant is obtained using boundary conditions given by equation (2.8), with the expressions for the spheroidal harmonics on $\xi = \xi_0$ being given by (2.9). One finds

$$A_x^t = \frac{U}{(3Q_0^0 - \xi_0 Q_1^0)}. \tag{3.2}$$

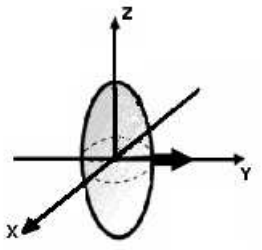


Figure 3.2: Prolate spheroid translating along Y-axis

The disturbance velocity field generated due to a prolate spheroid translating along the Y-axis with a velocity of magnitude U, as shown in figure 3.2, is given by

$$\mathbf{u}_y^t = A_y^t \left( \mathbf{S}_{1,1}^{(3)} + \mathbf{S}_{1,-1}^{(3)} \right). \tag{3.3}$$

The constant is again obtained using boundary conditions given by as mentioned in equation (2.8).

$$A_y^t = \frac{iU}{(\xi_0 Q_1^0 - 3Q_0^0)}. \tag{3.4}$$

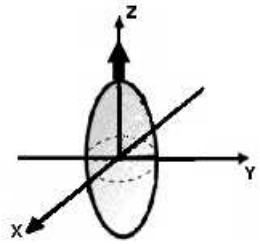


Figure 3.3: Prolate spheroid translating along Z-axis(the axis of symmetry)

The disturbance velocity field generated due to a prolate spheroid translating along its axis of symmetry, the Z-axis, with a velocity of magnitude U, as shown in figure 3.3, is given by

$$\mathbf{u}_z^t = A_z^t \left( \mathbf{S}_{1,0}^{(3)} \right). \tag{3.5}$$

The second index s, which is equal to zero in (3.5), indicates the axisymmetric nature of the velocity field.

Using (2.8) and (2.9), one finds,

$$A_z^t = \frac{U}{(\xi_0 Q_1^0 + Q_0^0)}. \tag{3.6}$$

The expressions for the disturbance velocity fields due to the translating spheroid were verified by comparison with the same velocity field obtained using the singularity method (Chwang & Wu (1975)), which employs a line distribution of Stokelets and potential doublets between the foci of the spheroid to generate the required disturbance velocity field in each case.

### 3.1.2 Disturbance velocity field due to a rotating spheroid

Herein, the disturbance velocity fields due to the rotation of a spheroid about the three independent Cartesian directions(x,y,z) are presented. Rotation about an arbitrary axis can be found by a suitable linear combination of the three canonical disturbance velocity fields.

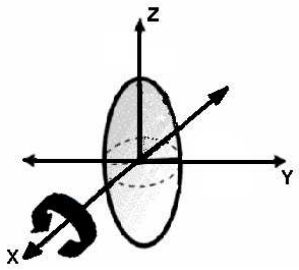


Figure 3.4: Prolate spheroid rotating about the X-axis

The disturbance velocity field generated due to a prolate spheroid rotating about the minor axis, X-axis, with angular velocity a magnitude W(as shown in figure 3.4) is given by

$$\mathbf{u}_x^r = A_{1x}^r \left( \mathbf{S}_{1,1}^{(3)} - \mathbf{S}_{1,-1}^{(3)} \right) + A_{2x}^r \left( \mathbf{S}_{2,1}^{(3)} + \mathbf{S}_{2,-1}^{(3)} \right). \tag{3.7}$$

The constants obtained using the boundary conditions in equation (2.8) and using equation (2.9) are,

$$A_{1x}^r = \frac{Wid(2\xi_0^2 - 1))}{(2\xi_0 Q_1^0 - \sqrt{\xi_0^2 - 1} Q_1^1)}, \tag{3.8}$$

$$A_{2x}^r = \frac{-Wid}{(2\xi_0 Q_1^0 - \sqrt{\xi_0^2 - 1} Q_1^1)}. \tag{3.9}$$

The disturbance velocity field generated due to a prolate spheroid rotating

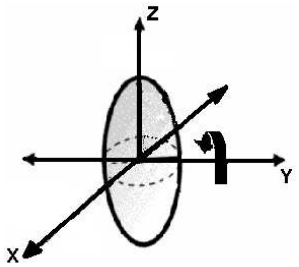


Figure 3.5: Prolate spheroid rotating about the Y-axis

about the Y-axis with angular velocity of magnitude W (as shown in figure 3.5) is given by

$$\mathbf{u}_y^r = A_{1y}^r \left( \mathbf{S}_{1,1}^{(3)} + \mathbf{S}_{1,-1}^{(3)} \right) + A_{2y}^r \left( \mathbf{S}_{2,1}^{(3)} - \mathbf{S}_{2,-1}^{(3)} \right). \tag{3.10}$$

The constants are obtained using the boundary conditions in equation (2.8).

$$A_{1y}^r = \frac{Wd(2\xi_0^2 - 1))}{(2\xi_0 Q_1^0 - \sqrt{\xi_0^2 - 1} Q_1^1)}, \tag{3.11}$$

$$\mathbf{A}_{2y}^r = \frac{Wd}{(2\xi_0 Q_1^0 - \sqrt{\xi_0^2 - 1} Q_1^1)}. \tag{3.12}$$

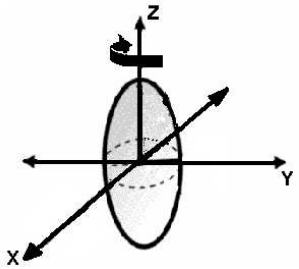


Figure 3.6: Prolate spheroid rotating about the Z-axis (axis of symmetry)

The disturbance velocity generated due to a prolate spheroid rotating about the

Z-axis, its axis of symmetry, with an angular velocity of magnitude W, as shown in figure 3.6, is given by

$$\mathbf{u}_z^r = A_z^r \left( \mathbf{S}_{1,0}^{(2)} \right) \tag{3.13}$$

The constant is again obtained using boundary conditions in equation (2.8) with the expressions for the spheroidal harmonics on $\xi = \xi_0$ being given by (2.9).

$$A_z^r = \frac{-2iWd\sqrt{\xi_0^2 - 1}}{Q_1^1} \tag{3.14}$$

### 3.1.3 Disturbance velocity field due to a spheroid immersed in ambient linear flows: Axisymmetric extension, Transverse extensions and Longitudinal extensions

Since the rate of strain tensor $\boldsymbol{E}$ is symmetric and traceless, an arbitrary extensional flow given by $\boldsymbol{u}^\infty = \boldsymbol{E}.x$ may be generated by a linear combination of axisymmetric extension, a pair of transverse extensions, and a pair of longitudinal extensions. The axisymmetric extension is the only 3-D flow amongst the five flows. Here, 'transverse' refers to the plane perpendicular to the axes of symmetry, and 'longitudinal' refers to the plane containing the axis of symmetry.

(1) The rate of strain tensor for an axisymmetric extension flow is given by $\boldsymbol{E}_{axi} = \begin{pmatrix} -k_1 & 0 & 0 \\ 0 & -k_1 & 0 \\ 0 & 0 & 2k_1 \end{pmatrix}$; here, $k_1$ denotes the strength of the straining velocity field. The disturbance velocity field generated due to a force-free, torque-free prolate spheroid placed in an axisymmetric extensional flow, as shown in figure 3.7,

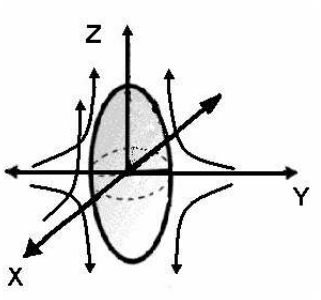


Figure 3.7: Prolate spheroid placed in an axisymmetric extensional flow

is given by

$$\mathbf{u}_{axi} = A_{axi}\left(\mathbf{S}^{(3)}_{2,0}\right). \tag{3.15}$$

The constant is obtained using boundary condition, $\mathbf{u}_{axi} = -(\boldsymbol{E}_{axi}.\boldsymbol{x})$, where $\boldsymbol{E}_{axi}$ is the rate of strain tensor for axisymmetric extension flow. One finds,

$$A_{axi} = \frac{k_1 2d\sqrt{\xi_0^2 - 1}}{(Q_1^1 - \xi_0 Q_2^1)}. \tag{3.16}$$

The above velocity field verified by comparison with the same velocity field obtained using the singularity method (Chwang & Wu (1975)). In the latter method a distribution of stresslets and potential quadrupoles between the foci was used to generate the required disturbance velocity field.

(2) The rate of strain tensor for a transverse extensional flow-1, with the axes of extension and compression along Y and X-axis respectively, (shown in figure 3.8 on the left) is given by

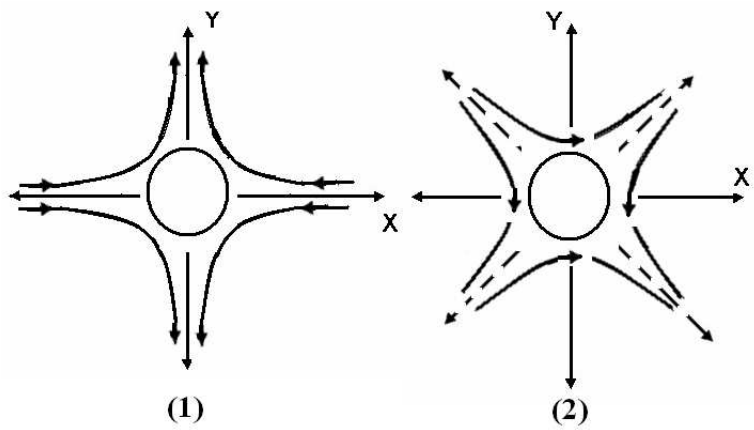


Figure 3.8: Prolate spheroid placed in a transverse extensional flow

$\boldsymbol{E}^1_{te}$=$\begin{pmatrix} -k_2 & 0 & 0 \\ 0 & k_2 & 0 \\ 0 & 0 & 0 \end{pmatrix}$; here, $k_2$ denotes the strength of the flow. The disturbance velocity field is given by

$$\mathbf{u}^1_{te} = A^1_{te}\left(\mathbf{S}^{(3)}_{2,2} + \mathbf{S}^{(3)}_{2,-2}\right). \tag{3.17}$$

The constant is obtained using the boundary condition $\mathbf{u}^1_{te} = -(\boldsymbol{E}^1_{te}.\boldsymbol{x})$, where $\boldsymbol{E}^1_{te}$ is the rate of strain tensor for transverse extension flow-1. One finds,

$$A^1_{te} = \frac{k_2 2d\sqrt{\xi_0^2 - 1}}{(\xi_0 Q^1_2 - 3Q^1_1)}. \tag{3.18}$$

(3) The rate of strain tensor for a transverse extensional flow-2, with the axis of extension and compression inclined at an angle $45^o$ to the X and Y-axes (as shown on the right of figure 3.8) is given by

$\boldsymbol{E}^2_{te} = \begin{pmatrix} 0 & k_3 & 0 \\ k_3 & 0 & 0 \\ 0 & 0 & 0 \end{pmatrix}$ ;here, $k_3$ denotes the strength of the flow. The disturbance velocity field is given by

$$\mathbf{u}^2_{te} = A^2_{te}\left(\mathbf{S}^{(3)}_{2,2} - \mathbf{S}^{(3)}_{2,-2}\right). \tag{3.19}$$

The constant is obtained using boundary condition $\mathbf{u}^2_{te} = -(\boldsymbol{E}^2_{te}.\boldsymbol{x})$, where $\boldsymbol{E}^2_{te}$ is the rate of strain tensor for transverse extension flow-2. One finds,

$$A^2_{te} = \frac{k_3 2id\sqrt{\xi_0^2 - 1}}{(3Q^1_1 - \xi_0 Q^1_2)}. \tag{3.20}$$

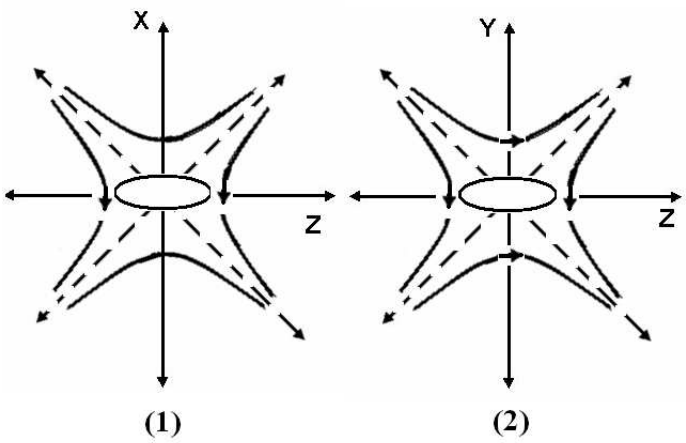


Figure 3.9: Prolate spheroid placed in a longitudinal extensional flow

(4) The rate of strain tensor for a longitudinal extensional flow-1, with the extension and compression occurring in the X-Z plane as shown on the right of figure 3.9, is given by

$\boldsymbol{E}^1_{le} = \begin{pmatrix} 0 & 0 & k_4 \\ 0 & 0 & 0 \\ k_4 & 0 & 0 \end{pmatrix}$ ;here, $k_4$ denotes the strength of the flow. The disturbance velocity field is given by

$$\mathbf{u}^1_{le} = A^1_{le}\left(\mathbf{S}^{(3)}_{2,1} - \mathbf{S}^{(3)}_{2,-1}\right). \tag{3.21}$$

The constant is obtained using the boundary condition $\mathbf{u}^1_{le} = -(\boldsymbol{E}^1_{le}.\boldsymbol{x})$, where $\boldsymbol{E}^1_{le}$ is the rate of strain tensor for longitudinal extensional flow-1. One finds,

$$A^1_{le} = \frac{k_4 d(\xi_0^2 - 1)}{2\xi_0(Q^0_1 - \xi_0 Q^0_2)}. \tag{3.22}$$

(5) The rate of strain tensor for a longitudinal extensional flow-2, with the extension and compression occurring in Y-Z plane as shown on the left of figure 3.9, is given by

$\boldsymbol{E}^2_{le} = \begin{pmatrix} 0 & 0 & 0 \\ 0 & 0 & k_5 \\ 0 & k_5 & 0 \end{pmatrix}$ , here $k_5$ denotes the strength of the flow. The disturbance velocity field is given by

$$\mathbf{u}^2_{le} = A^2_{le}\left(\mathbf{S}^{(3)}_{2,1} + \mathbf{S}^{(3)}_{2,-1}\right). \tag{3.23}$$

The constant is obtained using boundary condition $\mathbf{u}^2_{le} = -(\boldsymbol{E}^2_{le}.\boldsymbol{x})$, where $\boldsymbol{E}^2_{le}$ is the rate of strain tensor for longitudinal extensional flow-2. One finds,

$$A^2_{le} = \frac{k_5 i d(\xi_0^2 - 1)}{2\xi_0(Q^0_1 - \xi_0 Q^0_2)}. \tag{3.24}$$

The disturbance velocity field due to a prolate spheroid placed in a longitudinal

extensional flow is obtained using the singularity method (Chwang & Wu (1975)) for comparison. This may be done by superimposing a longitudinal shear flow past a prolate spheroid and a cross-flow with a longitudinal rate of shear past a prolate spheroid.

In a similar manner, the canonical velocity fields were obtained for an oblate spheroid too. The velocity can be expressed using the same linear combination of the partial vectorial solutions as given for a prolate spheroid. The partial vectorial solutions for an oblate spheroidal coordinate system are given in equation (2.10). But the constants obtained differ,and these are obtained using equations (2.11).

The disturbance velocity fields obtained for the various motions of a prolate spheroid, and in different ambient linear flows, with their corresponding constants have been tabulated below:

| | Motion | Velocity fields | Constants |
|---|---|---|---|
| 1 | X-axis translation | $\mathbf{A}_x^t \left(\mathbf{S}_{1,1}^{(3)} - \mathbf{S}_{1,-1}^{(3)}\right)$ | $\mathbf{A}_x^t = \frac{U}{(3Q_0^0 - \xi_0 Q_1^0)}$ |
| 2 | Y-axis translation | $\mathbf{u}_y^t = \mathbf{A}_y^t \left(\mathbf{S}_{1,1}^{(3)} + \mathbf{S}_{1,-1}^{(3)}\right)$ | $\mathbf{A}_y^t = \frac{iU}{(\xi_0 Q_1^0 - 3Q_0^0)}$ |
| 3 | Z-axis translation | $\mathbf{u}_z^t = \mathbf{A}_z^t \left(\mathbf{S}_{1,0}^{(3)}\right)$ | $\mathbf{A}_z^t = \frac{U}{(\xi_0 Q_1^0 + Q_0^0)}$ |
| 4 | Rotation about X-axis | $\mathbf{A}_{1x}^r \left(\mathbf{S}_{1,1}^{(3)} - \mathbf{S}_{1,-1}^{(3)}\right) + \mathbf{A}_{2x}^r \left(\mathbf{S}_{2,1}^{(3)} + \mathbf{S}_{2,-1}^{(3)}\right)$ | $\mathbf{A}_{1x}^r = \frac{Wid(2\xi_0^2 - 1))}{(2\xi_0 Q_1^0 - \sqrt{\xi_0^2 - 1} Q_1^1)}$<br>$\mathbf{A}_{2x}^r = \frac{-Wid}{(2\xi_0 Q_1^0 - \sqrt{\xi_0^2 - 1} Q_1^1)}$ |
| 5 | Rotation about Y-axis | $\mathbf{A}_{1y}^r \left(\mathbf{S}_{1,1}^{(3)} + \mathbf{S}_{1,-1}^{(3)}\right) + \mathbf{A}_{2y}^r \left(\mathbf{S}_{2,1}^{(3)} - \mathbf{S}_{2,-1}^{(3)}\right)$ | $\mathbf{A}_{1y}^r = \frac{Wd(2\xi_0^2 - 1))}{(2\xi_0 Q_1^0 - \sqrt{\xi_0^2 - 1} Q_1^1)}$<br>$\mathbf{A}_{2y}^r = \frac{Wd}{(2\xi_0 Q_1^0 - \sqrt{\xi_0^2 - 1} Q_1^1)}$ |
| 6 | Rotation about Z-axis | $\mathbf{A}_z^r \left(\mathbf{S}_{1,0}^{(2)}\right)$ | $\mathbf{A}_z^r = \frac{-2iWd\sqrt{\xi_0^2 - 1}}{Q_1^1}$ |
| 7 | Axisymmetric extensional flow | $\mathbf{A}_{axi} \left(\mathbf{S}_{2,0}^{(3)}\right)$ | $\mathbf{A}_{axi} = \frac{k_1 2d\sqrt{\xi_0^2 - 1}}{(Q_1^1 - \xi_0 Q_2^1)}$ |
| 8 | Transverse extensional flow-1 | $\mathbf{A}_{te}^1 \left(\mathbf{S}_{2,2}^{(3)} + \mathbf{S}_{2,-2}^{(3)}\right)$ | $\mathbf{A}_{te}^1 = \frac{k_2 2d\sqrt{\xi_0^2 - 1}}{(\xi_0 Q_2^1 - 3Q_1^1)}$ |
| 9 | Transverse extensional flow-2 | $\mathbf{A}_{te}^2 \left(\mathbf{S}_{2,2}^{(3)} - \mathbf{S}_{2,-2}^{(3)}\right)$ | $\mathbf{A}_{te}^2 = \frac{k_3 2id\sqrt{\xi_0^2 - 1}}{(3Q_1^1 - \xi_0 Q_2^1)}$ |
| 10 | Longitudinal extensional flow-1 | $\mathbf{A}_{le}^1 \left(\mathbf{S}_{2,1}^{(3)} - \mathbf{S}_{2,-1}^{(3)}\right)$ | $\mathbf{A}_{le}^1 = \frac{k_4 d(\xi_0^2 - 1)}{2\xi_0 (Q_1^0 - \xi_0 Q_2^0)}$ |
| 11 | Longitudinal extensional flow-2 | $\mathbf{A}_{le}^2 \left(\mathbf{S}_{2,1}^{(3)} + \mathbf{S}_{2,-1}^{(3)}\right)$ | $\mathbf{A}_{le}^2 = \frac{k_5 id(\xi_0^2 - 1)}{2\xi_0 (Q_1^0 - \xi_0 Q_2^0)}$ |

The velocity fields obtained for the corresponding motions of an oblate spheroid in different ambient flows have been tabulated below:

| | Motion | Velocity fields | Constants |
|---|---|---|---|
| 1 | X-axis translation | $\mathbf{A}_x^t \left(\mathbf{S}_{1,1}^{(3)} - \mathbf{S}_{1,-1}^{(3)}\right)$ | $\mathbf{A}_x^t = \frac{U}{(3Q_0^0 - i\sqrt{\xi_0^2-1}Q_1^0)}$ |
| 2 | Y-axis translation | $\mathbf{u}_y^t = \mathbf{A}_y^t \left(\mathbf{S}_{1,1}^{(3)} + \mathbf{S}_{1,-1}^{(3)}\right)$ | $\mathbf{A}_y^t = \frac{iU}{(i\sqrt{\xi_0^2-1}Q_1^0 - 3Q_0^0)}$ |
| 3 | Z-axis translation | $\mathbf{u}_z^t = \mathbf{A}_z^t \left(\mathbf{S}_{1,0}^{(3)}\right)$ | $\mathbf{A}_z^t = \frac{-U}{(i\sqrt{\xi_0^2-1}Q_1^0 + Q_0^0)}$ |
| 4 | Rotation about X-axis | $\mathbf{A}_{1x}^r \left(\mathbf{S}_{1,1}^{(3)} - \mathbf{S}_{1,-1}^{(3)}\right) + \mathbf{A}_{2x}^r \left(\mathbf{S}_{2,1}^{(3)} + \mathbf{S}_{2,-1}^{(3)}\right)$ | $\mathbf{A}1_x^r = \frac{id\left[i(\xi_0^2-1)Q_2^1 - \xi_0(2Q_1^0 - 2i\sqrt{\xi_0^2-1}Q_2^0)\right]}{2\left[i\sqrt{\xi_0^2-1}Q_1^0Q_2^1 + Q_1^1(Q_1^0 - i\sqrt{\xi_0^2-1}Q_2^0)\right]}$ <br> $\mathbf{A}2_x^r = \frac{id\left[\sqrt{\xi_0^2-1}Q_1^1 + 2\xi_0 Q_1^0\right]}{2\left[i\sqrt{\xi_0^2-1}Q_1^0Q_2^1 + Q_1^1(Q_1^0 - i\sqrt{\xi_0^2-1}Q_2^0)\right]}$ |
| 5 | Rotation about Y-axis | $\mathbf{A}_{1y}^r \left(\mathbf{S}_{1,1}^{(3)} + \mathbf{S}_{1,-1}^{(3)}\right) + \mathbf{A}_{2y}^r \left(\mathbf{S}_{2,1}^{(3)} - \mathbf{S}_{2,-1}^{(3)}\right)$ | $\mathbf{A}1_y^r = \frac{d\left[i(\xi_0^2-1)Q_2^1 - \xi_0(2Q_1^0 - 2i\sqrt{\xi_0^2-1}Q_2^0)\right]}{2\left[i\sqrt{\xi_0^2-1}Q_1^0Q_2^1 + Q_1^1(Q_1^0 - i\sqrt{\xi_0^2-1}Q_2^0)\right]}$ <br> $\mathbf{A}2_y^r = \frac{d\left[\sqrt{\xi_0^2-1}Q_1^1 + 2\xi_0 Q_1^0\right]}{2\left[i\sqrt{\xi_0^2-1}Q_1^0Q_2^1 + Q_1^1(Q_1^0 - i\sqrt{\xi_0^2-1}Q_2^0)\right]}$ |
| 6 | Rotation about Z-axis | $\mathbf{A}_z^r \left(\mathbf{S}_{1,0}^{(2)}\right)$ | $\mathbf{A}_z^r = \frac{2iWd\xi_0}{Q_1^1}$ |
| 7 | Axisymmetric extensional flow | $\mathbf{A}_{axi} \left(\mathbf{S}_{2,0}^{(3)}\right)$ | $\mathbf{A}_{axi} = \frac{k_1 2d\xi_0}{(i\sqrt{\xi_0^2-1}Q_2^1 - Q_1^1)}$ |
| 8 | Transverse extensional flow-1 | $\mathbf{A}_{te}^1 \left(\mathbf{S}_{2,2}^{(3)} + \mathbf{S}_{2,-2}^{(3)}\right)$ | $\mathbf{A}_{te}^1 = \frac{k_2 2d\xi_0}{(3Q_1^1 - i\sqrt{\xi_0^2-1}Q_2^1)}$ |
| 9 | Transverse extensional flow-2 | $\mathbf{A}_{te}^2 \left(\mathbf{S}_{2,2}^{(3)} - \mathbf{S}_{2,-2}^{(3)}\right)$ | $\mathbf{A}_{te}^2 = \frac{k_3 2id\xi_0}{(3Q_1^1 - i\sqrt{\xi_0^2-1}Q_2^1)}$ |
| 10 | Longitudinal extensional flow-1 | $\mathbf{A}_{le}^1 \left(\mathbf{S}_{2,1}^{(3)} - \mathbf{S}_{2,-1}^{(3)}\right)$ | $\mathbf{A}_{le}^1 = \frac{-k_4 2id\xi_0\sqrt{\xi_0^2-1)}}{Q_2^1(2(\xi_0^2-1)+1)}$ |
| 11 | Longitudinal extensional flow-2 | $\mathbf{A}_{le}^2 \left(\mathbf{S}_{2,1}^{(3)} + \mathbf{S}_{2,-1}^{(3)}\right)$ | $\mathbf{A}_{le}^2 = \frac{-2k_5 id\xi_0\sqrt{\xi_0^2-1)}}{Q_2^1(2(\xi_0^2-1)+1)}$ |

## 3.2 Results

In this section we discuss the analytical results for the torque obtained using the generalised reciprocal identity (2.23), and the expressions for the disturbance velocity fields derived in the previous section. We shall first present the results for the sedimentation problem. The results for the inertial and viscoelastic torques will be presented, and then the motion under the the combined effects of both these torques will be discussed. The results obtained thus far for the simple shear flow problem will also be discussed thereafter.

### 3.2.1 Spheroid sedimenting in a quiescent second-order fluid

#### Inertial torque acting on a spheroidal particle sedimenting in a quiescent second-order fluid

The total torque acting on the sedimenting particle is given by

$$\boldsymbol{L}_{sed} = Re \int_V \left( \frac{D\mathbf{u}^{(1)}}{Dt} \right) \boldsymbol{.u^{(2)}} dV + De \int_V \boldsymbol{\sigma^{(1)}_{NN}} \boldsymbol{:} \nabla \boldsymbol{u^{(2)}} dV. \tag{3.25}$$

The inertial torque has been found by evaluating the expression: $Re \int_V \left( \frac{D\boldsymbol{u}^{(1)}}{Dt} \right) \boldsymbol{.u^{(2)}} dV$, where $\frac{D\mathbf{u}^{(1)}}{Dt}$ is the acceleration of the disturbance velocity as observed from the body-fixed coordinate system translating with velocity $\boldsymbol{U}_1$ and is defined as $\boldsymbol{u}^{(1)}\boldsymbol{.\nabla u}^{(1)}$. Here, $\boldsymbol{u}^{(1)}$ is the disturbance velocity in the body-fixed coordinate system translating with velocity $\boldsymbol{U}_1$, and is defined as $\boldsymbol{u}^{(1)'} - \boldsymbol{U}_1$, where $\boldsymbol{u}^{(1)'}$ is the disturbance velocity observed from the lab frame of reference. $\boldsymbol{u}^{(1)'}$ can be written as the sum of the x-axis and z-axis translation disturbance velocity fields . The latter velocity fields can be found in the previous section [see equations (3.1) & (3.5)].

$$\boldsymbol{u}^{(1)'} = A_z \left( \mathbf{S}^{(3)}_{1,0} \right) + A_x \left( \mathbf{S}^{(3)}_{1,1} - \mathbf{S}^{(3)}_{1,-1} \right), \tag{3.26}$$

where $A_z = \left( \frac{U_1 \cos\alpha}{(\xi_0 Q^0_1 + Q^0_0)} \right)$, $A_x = \left( \frac{U_1 \sin\alpha}{(3Q^0_0 - \xi_0 Q^0_1)} \right)$ and $\boldsymbol{U}_1$ is the velocity of translation of the spheroid given by $(U_1 \sin\alpha)\boldsymbol{e}_x + (U_1 \cos\alpha)\boldsymbol{e}_z$. $\alpha$ is the angle between the translational velocity $\boldsymbol{U}_1$ and axis of symmetry of the spheroidal particle.

The velocity field of the test problem $\boldsymbol{u^{(2)}}$ is the disturbance velocity due to a spheroid rotating about the y-axis rotation [see (3.3)], with the magnitude of angular velocity equal to unity, and is given by

$$\boldsymbol{u}^{(2)} = A_{1y}\left(\mathbf{S}^{(3)}_{1,1} + \mathbf{S}^{(3)}_{1,-1}\right) + A_{2y}\left(\mathbf{S}^{(3)}_{2,1} - \mathbf{S}^{(3)}_{2,-1}\right), \tag{3.27}$$

where $A_{1y} = \frac{d(2\xi_0^2-1))}{(2\xi_0 Q_1^0 - \sqrt{\xi_0^2-1}Q_1^1)}$ and $A_{2y} = \frac{d}{(2\xi_0 Q_1^0 - \sqrt{\xi_0^2-1}Q_1^1)}$.

Using the above expressions for the disturbance velocity fields, and the inertial acceleration, the $O(Re)$ inertial torque on a sedimenting spheroid is:

$$Re\left(\mu L^2 U\right) L_{sed(inertial)} \sin 2\alpha, \tag{3.28}$$

where $L_{sed(inertial)}$ for a prolate spheroid is given by

$$\begin{aligned} L_{sed(inertial)} = & \quad \frac{-\pi e^2\left(420e + 2240e^3 + 4249e^5 - 2152e^7\right)}{315((e^2+1)\tanh^{-1}e - e)^2((1-3e^2)\tanh^{-1}e - e)} \\ & + \quad \frac{\pi e^2\left(420 + 3360e^2 + 1890e^4 - 1470e^6\right)\tanh^{-1}e}{315((e^2+1)\tanh^{-1}e - e)^2((1-3e^2)\tanh^{-1}e - e)} \\ & - \quad \frac{\pi e^2\left(1260e - 1995e^3 + 2730e^5 - 1995e^7\right)(\tanh^{-1}e)^2}{315((e^2+1)\tanh^{-1}e - e)^2((1-3e^2)\tanh^{-1}e - e)}, \end{aligned} \tag{3.29}$$

and $L_{sed(inertial)}$ for an oblate spheroid is given by

$$\begin{aligned} L_{sed(inertial)} = & \quad \frac{\pi e^3\sqrt{1-e^2}\left(-420 + 3500e^2 - 9989e^4 + 4757e^6\right)}{315\sqrt{1-e^2}(-e\sqrt{1-e^2} + \sin^{-1}e + 2e^2\sin^{-1}e)(e\sqrt{1-e^2} + (2e^2-1)\sin^{-1}e)^2} \\ & + \quad \frac{210\pi e^2\left(2 - 24e^2 + 69e^4 - 67e^6 + 20e^8\right)\sin^{-1}e}{315\sqrt{1-e^2}(-e\sqrt{1-e^2} + \sin^{-1}e + 2e^2\sin^{-1}e)(e\sqrt{1-e^2} + (2e^2-1)\sin^{-1}e)^2} \\ & + \quad \frac{105\pi e^3\sqrt{1-e^2}\left(12 - 17e^2 + 24e^4\right)(\sin^{-1}e)^2}{315\sqrt{1-e^2}(-e\sqrt{1-e^2} + \sin^{-1}e + 2e^2\sin^{-1}e)(e\sqrt{1-e^2} + (2e^2-1)\sin^{-1}e)^2}. \end{aligned} \tag{3.30}$$

(We have obtained all our analytical expressions as a function of the particle eccentricity e. The particle eccentricity e is defined as $e = \frac{1}{\xi_0}$. As $e \to 0$ we obtain

a sphere and as $e \rightarrow 1$ we obtain a rod in case of a prolate spheroid and a disc in case of an oblate spheroid)

The above analytical expressions were obtained using the symbolic computing tool, Wolfram Mathematica-6.

Our analytical results for the inertial torque on a prolate spheroid of an arbitrary aspect ratio did match with numerical values given by G.P.Galdi *et al.* (2002), who used the singularity method developed for the Stokes flows by Chwang and Wu (T.Chwang & Wu (1974) and Chwang & Wu (1975)) to calculate the disturbance velocity fields, and further, did a numerical integration to find out the inertial torque acting on the prolate spheroid.

In the limit of a slender fiber, that is, when $\xi_0 \rightarrow 1$, the expression for the inertial torque acting on a prolate spheroid matched with the $O(Re)$ inertial torque acting on the sedimenting fiber given by Khayat and Cox in the limit of small $Re$ [see Cox (1989)]. An alternate, more succinct method of obtaining this torque has been given in Subramanian & Koch (2005). The limiting inertial torque acting on the fiber is given by

$$L_{sed(inertial)} = Re \frac{-10\pi}{3\left(ln(\xi_0 - 1)\right)^2} \mu U L^2 \sin\left(2\alpha\right),$$

where $\alpha$ is the angle the axis of the fiber makes with the direction of translation.

In all the above expressions the trigonometric factor $\sin\left(2\alpha\right)$ implies that there exists only two equilibrium orientations $\alpha = 0^o$ and $\alpha = 90^o$. $\alpha = 0^o$ is an unstable equilibrium and fluid inertia causes the fiber to orient at $\alpha = 90^o$, that is, the particle aligns with its axis of symmetry perpendicular to the direction of translation. Our analytical result in the limit of a spheroid of small eccentricity matched with what has been reported in Cox (1965) [see equation (1.4)], but with a slight numer-

ical discrepancy. We obtained the inertial torque on a spheroid of small eccentricity to be:

$$\boldsymbol{L}_{\boldsymbol{sed(inertial)}} = Re\frac{811\pi}{1120}\epsilon\mu U L^2 \sin 2\alpha. \tag{3.31}$$

In our notation dimensionless measure of the departure from sphericity ($\epsilon$) is given by $\epsilon=\frac{1}{2\xi_0^2}$.

The inertial torque given in equation (3.28), characterized by the Reynolds number, turns the spheroid in a direction which offers maximum resistance to flow, that is, the spheroid turns broadside on. In other words, the axis of symmetry of a prolate spheroid turns in a direction perpendicular to the direction of translation and the axis of symmetry of an oblate spheroid orients along the direction of translation.

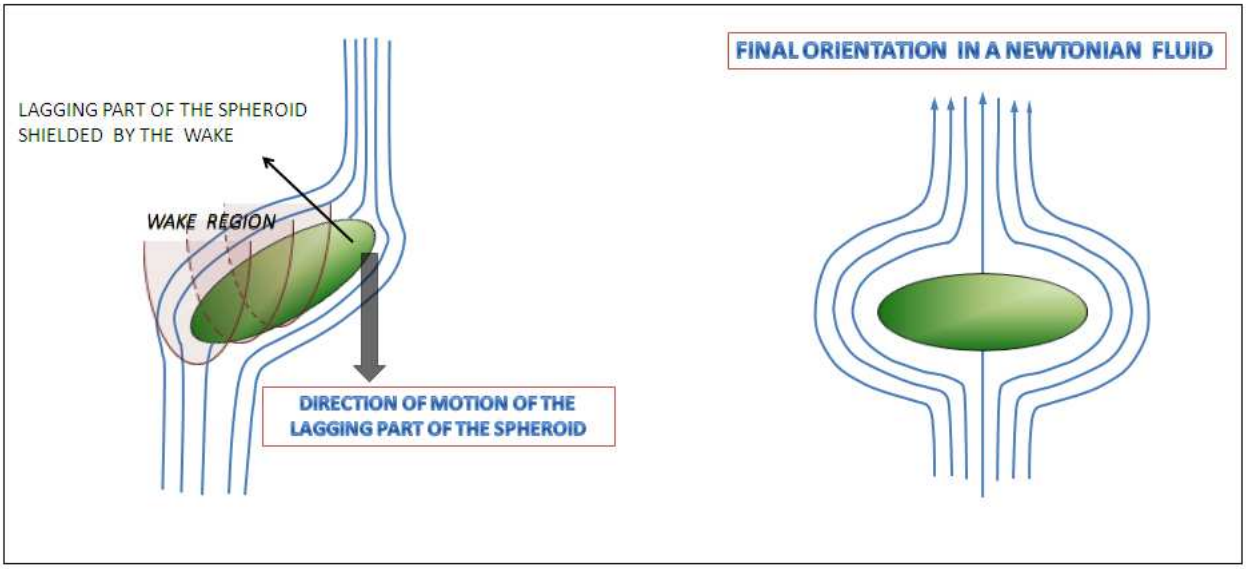


Figure 3.10: The effect of inertia on a sedimenting prolate spheroid

Figure 3.10 shows a prolate spheroid turning broadside on in a Newtonian fluid as the wake of the leading part of the spheroid shields the lagging part of the spheroid. The lagging part of the spheroid does not feel the full force of the incoming flow. Hence the spheroid rotates until the lagging part catches up with

the leading part of the body, making the whole spheroid turn in the direction indicated in figure 3.10. Note that the depiction of the mechanism is intended to be strictly qualitative, since for small $Re$, the wake of the particle begins only at a distance of $O((d\xi_0)Re^{-1})$, the inertial screening length, behind it.

### Viscoelastic torque acting on a spheroidal particle sedimenting in a quiescent second-order fluid

The viscoelastic torque acting on a sedimenting spheroidal particle has been found by evaluating the expression: $De\int_V \boldsymbol{\sigma}^{(1)}_{NN} : \nabla \boldsymbol{u}^{(2)} dV$ in equation (3.25). Here, $\boldsymbol{\sigma}^{(1)}_{NN}$ is the non-Newtonian stress due to the disturbance velocity field $\boldsymbol{u}^{(1)}$ in the actual problem, and $\boldsymbol{u}^{(2)}$ is the disturbance velocity field in the test problem.

The analytical expression for the $O(De)$ viscoelastic torque acting on a sedimenting spheroid is given by $De(\mu L^2 U)L_{sed(visco)} \sin 2\alpha$, where $L_{sed(visco)}$ for a prolate spheroid is given by

$$\begin{aligned} L_{sed(visco)} = & \quad \frac{8\pi e^3 \epsilon_1 \left(-3e - (e^2+3)\tanh^{-1} e\right)}{\left(e - (e^2+1)\tanh^{-1} e\right)\left((3e^2-1)\tanh^{-1} e + e\right)} \\ + & \quad \frac{16\pi e^3(\epsilon_1+1)\left(6e^2 - 64e^4 + (6e - 26e^3)\tanh^{-1} e + (13e^4 - 6e^2 - 3)\left(\tanh^{-1} e\right)^2\right)}{\left(e - (e^2+1)\tanh^{-1} e\right)^2\left((3e^2-1)\tanh^{-1} e + e\right)}, \end{aligned} \tag{3.32}$$

and $L_{sed(visco)}$ for an oblate spheroid is given by

$$\begin{aligned} L_{sed(visco)} = & \frac{-8\pi e^3 \epsilon_1 (3e\sqrt{1-e^2} + (2e^2-3)\sin^{-1} e)}{e^2(e^2-1) + 2e\sqrt{1-e^2}(\sin^{-1} e) + (4e^2-1)(\sin^{-1})^2} \\ & + \\ & \frac{16\pi e^3(1+\epsilon_1)\left(29e^4 + 3e^2 - 2e\sqrt{1-e^2}(10e^2+3)\sin^{-1} e - (4e^4 + 12e^2 - 3)(\sin^{-1} e)^2\right)}{\left(e\sqrt{1-e^2} + (2e^2-1)\sin^{-1} e\right)^2\left(e\sqrt{1-e^2} - (2e^2+1)\sin^{-1} e\right)}. \end{aligned} \tag{3.33}$$

The sense of the viscoelastic torque is to rotate the spheroidal particle into an orientation that offers minimum resistance to flow. Here, the terminal orientations are exactly opposite of what inertia would do.

Leal (1975) found the torque acting on slender fiber in a second-order fluid to be: $L_{sed(visco)} = K \sin 2\alpha$, where K is the torque coefficient, given by

$$K = De \left( \frac{\mu U L^2 \pi}{-32(lnA_r)^3} \right) \int_{-1+r}^{1-r} dx_1 \int_{R(x_1)}^{c_1} r dr \left[ \frac{x_1^2}{r^2} \left( ln \frac{r^2}{4(1-x_1^2)} \right)^2 \right] (96\epsilon_1 - 16) .$$

Here, $A_r$ is the aspect ratio of the particle, which in our notation is denoted by $\left( \frac{\xi_0}{\sqrt{\xi_0^2 - 1}} \right)$, $\epsilon_1$ is related to the ratio of the normal stress coefficients and the co-ordinate system$(x_1, x_2, x_3)$ are fixed in the particle, such that $x_1$ is aligned along the axis of symmetry of the particle and $R(x_1)$ is $\sqrt{x_2^2 + x_3^2}$ for a spheroidal particle. Leal reported that the torque coefficient is strictly negative, implying that the torque will align the axis of symmetry of the particle with the direction of translation. We computed the torque coefficient K, and found it to be:

$$K = De \left( \frac{-\pi}{36} (16 - 96\epsilon_1) \right) \mu U L^2$$

This result, unlike ours, does not tend to zero in the limit $A_r \to \infty$ (a fiber with an asymptotically large aspect ratio). Leal's result appears to be erroneous since an infinitely long fiber has no finite surface area for the fluid stresses to act on. Hence one expects there to be no net torque to act on a infinitely slender fiber.

Galdi and his co-workers [see G.P.Galdi *et al.* (2002)] have reported that the viscoelastic torque changes sign for e at approximately 0.9 for $\epsilon_1 = -1.25, -1.42$ ($\epsilon_1$ is related to the ratio the normal stress coefficients). This is unlike our results, which do not show any sign reversal for any value of $\epsilon_1$. This error can perhaps

be ascribed to the extreme steepness of the viscoelastic torque curve [see figure (3.12)] near the slender fiber limit (e→1). This extreme steepness may make any numerical calculation prone to error.

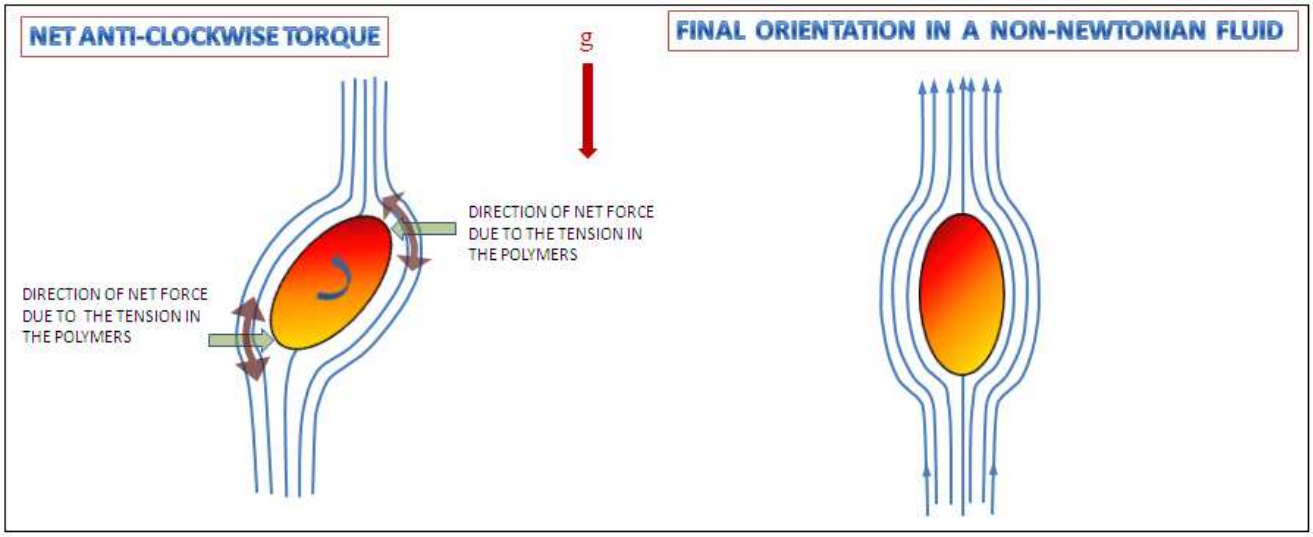


Figure 3.11: The effect of viscoelasticity on a sedimenting prolate spheroid

Figure 3.11 shows a prolate spheroid turning longside on due to fluid viscoelasticity. The polymer molecules in the fluid align themselves along the streamlines. The partially-aligned polymers molecules make the streamlines behave like stretched rubber bands. The tension in the streamlines is responsible for producing a net torque on the spheroid which makes it rotate into an orientation parallel to the direction of translation as shown in figure 3.11.

The other noteworthy features of the inertial and viscoelastic torques is that they vanish as the spheroids (both oblate and prolate) tend to a sphere, that is, as $e \to 0$ ($\xi_0 \to \infty$) [see figures 3.12 & 3.14]. This is because an isotropic object such as a sphere cannot experience any torque when sedimenting in an unbounded fluid. As already discussed earlier in the context of Leal's calculation, both the inertial and viscoelastic torques also vanish in the limit of a slender rod or a fiber ($e \to 1$

or $\xi_0 \to 1$). An infinite aspect ratio fiber does not have a finite area for the stress, either inertial or viscoelastic, to act on. Hence, it cannot experience any torque due to the fluid stresses. In the case of an oblate spheroid, as $e \to 1$ ($\xi_0 \to 1$), the spheroid approaches a disc, which has a finite area. Hence, the infinitely thin disc continues to experience a finite inertial and viscoelastic torque.

Further, as can be seen from figure 3.13, as the prolate spheroid tends to a fiber the viscoelastic torque becomes dominant compared to the inertial torque. The inertial torque decays as $O\Big(\frac{1}{(\log(1-e))^2}\Big)$, where as the viscoelastic torque decays as $O\Big(\frac{1}{\log(1-e)}\Big)$ in the limit $e \to 1$. The rate of decay of the inertial torque compared to the viscoelastic torque is faster by a factor of $O\Big(\frac{1}{\log(1-e)}\Big)$ in the limit $e \to 1$. As a result, the viscoelastic torque will always dominate over the inertial torque on a sufficiently slender fiber, and such a fiber will always orient parallel to the direction of translation.

### Neutral curve: competing inertial and viscoelastic torques

Since the inertial and viscoelastic torques act in opposite directions for both prolate and oblate spheroids as seen in figures 3.12 and 3.14, a balance of the two leads to a neutral curve, a critical value of De/Re as a function of the particle aspect ratio that separates regions where transverse and longitudinal orientations, respectively, are stable. Since we have the analytical expressions [see equations (3.29), (3.30), (3.32) & (3.33)] for the total torque on an arbitrary aspect ratio spheroid, we can obtain a neutral curve from the ratio of the inertial and the viscoelastic torques.

The ratio De/Re tends to zero as the prolate spheroid tends to a slender fiber ($e \to 1$), indicating, as discussed earlier, that in the limit of a slender fiber the viscoelastic torque dominates the inertial torque [see figure 3.13]. On the other

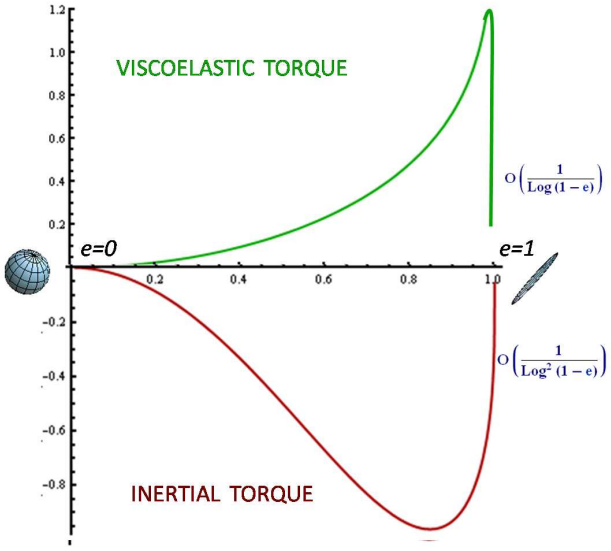


Figure 3.12: Inertial and viscoelastic torque on prolate spheroid

hand, De/Re tends to a finite constant as the oblate spheroid tends to a disc($e \to 1$) because the inertial and viscoelastic torques have finite values in this limit ($e \to 1$) [see figure 3.15]. De/Re also tends to a finite constant as the spheroid (prolate or oblate) tends to a sphere, since both the inertial and viscoelastic torques decay as $O(e^2)$ in the limit $e \to 0$.

### 3.2.2 Spheroid rotating in a simple shear flow

The inertialess trajectories of a spheroid placed in a simple shear flow are known as Jeffery orbits, and are governed by the following equations:

$$\begin{aligned} \frac{d\phi}{dt} &= \frac{\dot{\gamma}}{{A_r}^2+1}({A_r}^2\cos^2\phi + \sin^2\theta), \\ \frac{d\theta}{dt} &= \frac{\dot{\gamma}}{4}\left(\frac{{A_r}^2-1}{{A_r}^2+1}\right)\sin 2\theta \sin 2\phi, \end{aligned} \tag{3.34}$$

where, $A_r$ is the aspect ratio of the spheroid, and is defined as: $A_r = \frac{\xi_0}{\sqrt{\xi_0^2-1}}$ for a

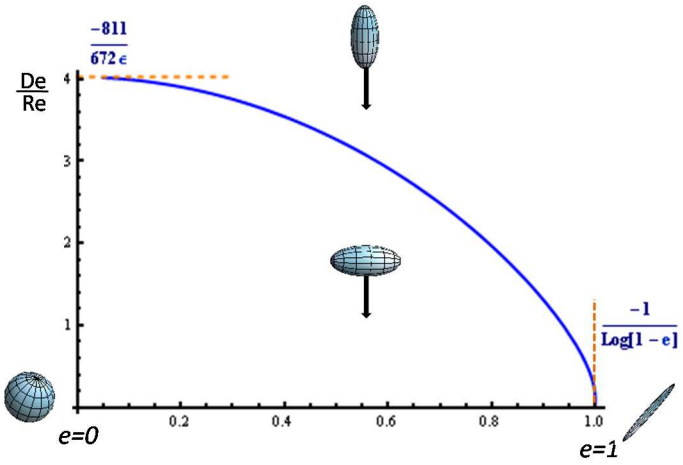


Figure 3.13: Neutral curve for a prolate spheroid

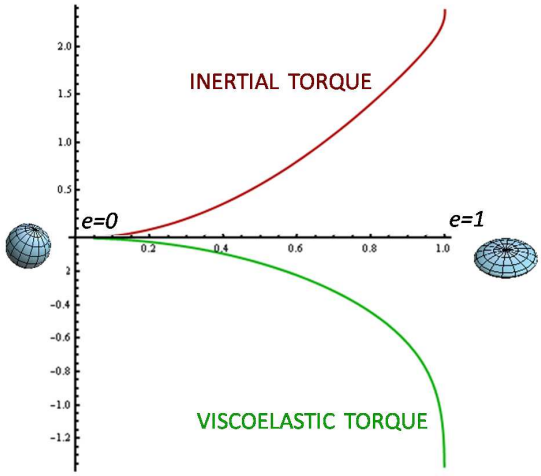


Figure 3.14: Inertial and viscoelastic torque on oblate spheroid

prolate spheroid and $A_r = \frac{\sqrt{\xi_0^2-1}}{\xi_0}$ for an oblate spheroid. Here $\theta$ and $\phi$ are defined, with respect to the vorticity direction as the polar and azimuthal angle respectively.

The Jeffery orbit equations are often defined in a more natural coordinate system of ($C$,$\tau$). The coordinate transformation from ($C$,$\tau$) to ($\theta$,$\phi$) are:

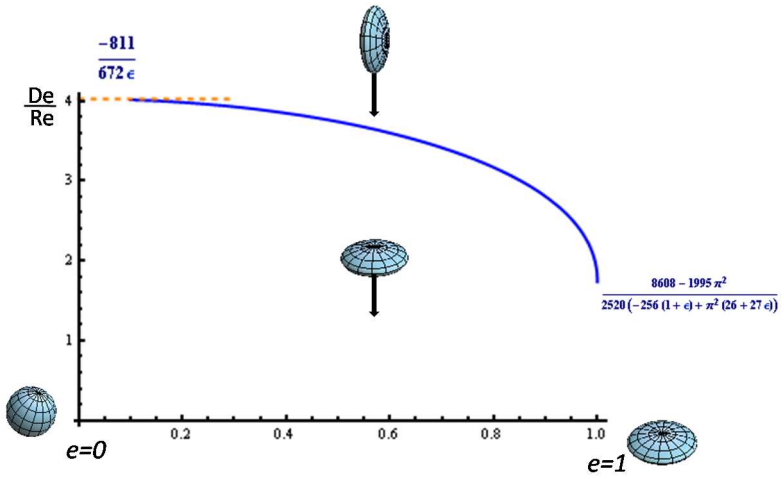


Figure 3.15: Neutral curve for an oblate spheroid

$$\theta = \tan^{-1}\left(C\sqrt{\cos^2\tau + {A_r}^2\sin^2\tau}\right),$$
$$\phi = \tan^{-1}\left(\tan A_r\tau\right), \tag{3.35}$$

where $C$ is the orbit constant and $\tau$ indicates the phase of the particle in the orbit. The Jeffery orbits of a arbitrary aspect ratio prolate spheroid is shown in figure 3.16.

The equations of motion in this coordinate system becomes:

$$\frac{dC}{dt} = 0, \tag{3.36}$$
$$\frac{d\tau}{dt} = \frac{A_r\dot{\gamma}}{{A_r}^2 + 1}. \tag{3.37}$$

The above equation shows that the orbit constant C, does not change with time, meaning that the particle will continue to rotate in the orbit which it was initially at. Thus, the particle does not drift across Jeffery orbits when fluid inertia or

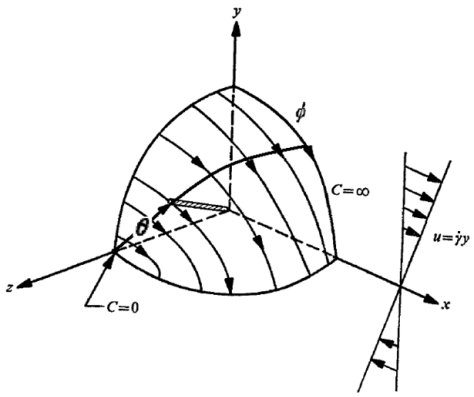


Figure 3.16: Jeffery orbits of a arbitrary aspect ratio prolate spheroid

viscoelasticity are absent (the Stokes limit). $C$ ranges from 0 to $\infty$. $C$=0 represents a log-rolling motion along the ambient vorticity axis, and $C$=$\infty$ represents a tumbling motion in the flow gradient plane. As the particle aspect ratio is varied from $A_r = 1$ to $A_r = \infty$ (sphere to a infinitely slender fiber), the projection of the Jeffery orbits on the flow-gradient plane changes from a circles to highly skewed ellipses. In the limit of infinite aspect ratio, the Jeffery orbits approach meridional trajectories running from one pole to the other, where the poles are the points of intersection of the flow axis with the unit circle [see figure 3.17].

The time period of rotation $T$ is given as:

$$T = \frac{2\pi}{\dot{\gamma}} \left( A_r + \frac{1}{A_r} \right).$$

Hence, a fiber of large aspect-ratio ($A_r >> 1$) spends a relatively long time aligned within the flow-vorticity plane, where the torque is small, it rotates away from the plane for a small time and flips rapidly until it becomes nearly aligned again.

When we apply the reciprocal theorem identity (2.23) we find that the angular velocity of a neutrally buoyant spheroid placed in a simple shear flow is governed

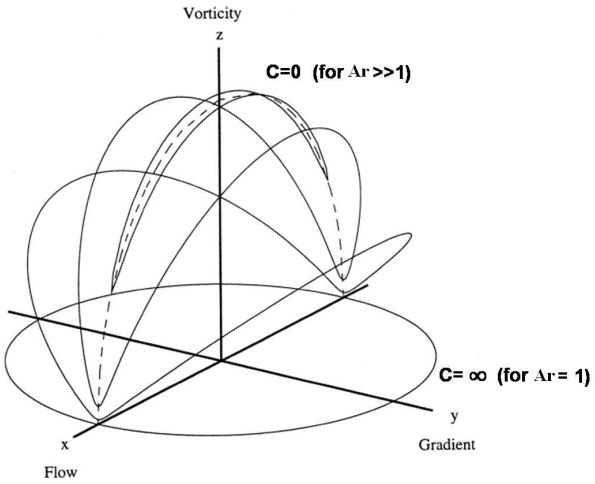


Figure 3.17: Jeffery orbits for various aspect ratio prolate spheroids

by a first-order differential equation, given by

$$St\left(\boldsymbol{I}_{sp}.\frac{d\boldsymbol{W}_{shear}}{dt}\right).\boldsymbol{w}_2-\boldsymbol{W}_{\boldsymbol{shear}}.\boldsymbol{L}_2=-\int_{S_p}(\boldsymbol{\Gamma}.\boldsymbol{x})\,.\left(\boldsymbol{\sigma}^{(2)}.\boldsymbol{n}\right)dS+Re\int_V \boldsymbol{f}.\boldsymbol{u}^{(2)}dV+De\int_V \boldsymbol{\sigma}^{(1)}_{NN}:\nabla\boldsymbol{u}^{(2)}dV. \tag{3.38}$$

Here, $\boldsymbol{f}$ is the acceleration associated with the disturbance velocity field $\boldsymbol{u}^{(1)'}$. $\boldsymbol{f}=\frac{\partial \boldsymbol{u}^{(1)'}}{\partial t}+\boldsymbol{\Gamma}.\boldsymbol{u}^{(1)'}+(\boldsymbol{\Gamma}.\boldsymbol{r}).\boldsymbol{\nabla}\boldsymbol{u}^{(1)'}+\boldsymbol{u}^{(1)'}.\boldsymbol{\nabla}\boldsymbol{u}^{(1)'}$. To find the Stokes disturbance velocity field $\boldsymbol{u}^{(1)'}$ induced by a neutrally buoyant spheroid in a simple shear flow, we first transform the strain rate tensor from the space fixed coordinate system (x,y,z) to a body fixed coordinate system $(x_b, y_b, z_b)$ [see figure 3.18]. To obtain the body-fixed coordinate system we rotate the space fixed coordinate system by an angle $\theta_j$ and $\phi_j$ as shown in the figure 3.18. The z-axis of the body-fixed coordinate system is aligned with the axis of symmetry of the spheroidal particle. Further, the y-axis of the body-fixed coordinate system is chosen to lie in the flow-gradient plane. Note that the transformation to the body-fixed coordinate is time dependent. In other words, $\theta_j$ and $\phi_j$ are functions of time, their evolution being governed, at leading order, by the Jeffery orbit equations [see equation(3.34)].

In this body-fixed coordinate system, we decompose the strain rate tensor into five independent parts. This is because the rate of strain tensor, being symmetric and traceless, has only five independent components. The Stokes disturbance velocity field due to each part is found, and these pieces are summed up to find the total disturbance velocity field due to the spheroidal particle rotating in a simple shear flow. Each of these five parts correspond to the five canonical ambient flows discussed in §3.1.3. Since we are assuming that $Re$ and $De$ are small, the resulting Stokes disturbance velocity field is sufficient when calculating the volume integrals.

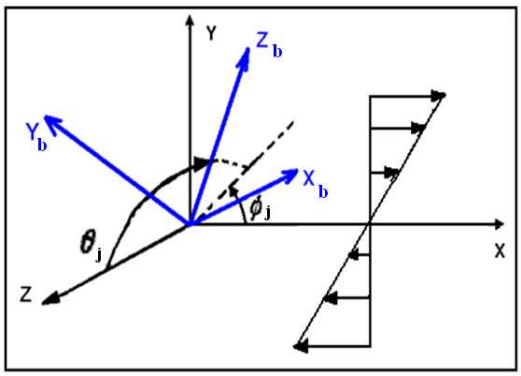


Figure 3.18: Coordinate rotation: from space-fixed$(x, y, z)$ to a body fixed coordinate system $(x_b, y_b, z_b)$

The transpose of the velocity gradient tensor for simple shear flow in body-fixed coordinates takes the form:

$$\mathbf{\Gamma}_{body}=\begin{pmatrix} \cos^2\theta_j \sin\phi_j \cos\phi_j & \frac{\cos\theta_j \cos^2\phi_j}{2} & \sin\theta_j \cos\theta_j \sin\phi_j \cos\phi_j \\ -\cos\theta_j \sin^2\phi_j & -\sin\phi_j \cos\phi_j & -\sin\theta_j \sin^2\phi_j \\ \sin\theta_j \cos\theta_j \sin\phi_j \cos\phi_j & \sin\theta_j \cos^2\phi_j & \sin^2\theta_j \sin\phi_j \cos\phi_j \end{pmatrix},$$

and the strain rate tensor for simple shear flow in body-fixed coordinates takes the form:

$$\boldsymbol{E}_{body}=\begin{pmatrix} \cos^2\theta_j \sin\phi_j \cos\phi_j & \frac{\cos\theta_j \cos 2\phi_j}{2} & \sin\theta_j \cos\theta_j \sin\phi_j \cos\phi_j \\ \frac{\cos\theta_j \cos 2\phi_j}{2} & -\sin\phi_j \cos\phi_j & \frac{\sin\theta_j \cos 2\phi_j}{2} \\ \sin\theta_j \cos\theta_j \sin\phi_j \cos\phi_j & \frac{\sin\theta_j \cos 2\phi_j}{2} & \sin^2\theta_j \sin\phi_j \cos\phi_j \end{pmatrix}$$

The above strain rate tensor may now be decomposed into five parts, as shown below:

$$\boldsymbol{E}_{body}=\boldsymbol{E}_{body-1}+\boldsymbol{E}_{body-2}+\boldsymbol{E}_{body-3}+\boldsymbol{E}_{body-4}+\boldsymbol{E}_{body-5}$$

where,

$$\boldsymbol{E}_{body-1}=\begin{pmatrix} \frac{-\sin^2\theta_j \sin\phi_j \cos\phi_j}{2} & 0 & 0 \\ 0 & \frac{-\sin^2\theta_j \sin\phi_j \cos\phi_j}{2} & 0 \\ 0 & 0 & \sin^2\theta_j \sin\phi_j \cos\phi_j \end{pmatrix},$$

$$\boldsymbol{E}_{body-2}=\begin{pmatrix} \frac{\cos^2\theta_j \sin\phi_j \cos\phi_j+\sin\phi_j \cos\phi_j}{2} & 0 & 0 \\ 0 & -\left(\frac{\cos^2\theta_j \sin\phi_j \cos\phi_j+\sin\phi_j \cos\phi_j}{2}\right) & 0 \\ 0 & 0 & 0 \end{pmatrix},$$

$$\boldsymbol{E}_{body-3}=\begin{pmatrix} 0 & \frac{\cos\theta_j \cos 2\phi_j}{2} & 0 \\ \frac{\cos\theta_j \cos 2\phi_j}{2} & 0 & 0 \\ 0 & 0 & 0 \end{pmatrix},$$

$$\boldsymbol{E}_{body-4}=\begin{pmatrix} 0 & 0 & \sin\theta_j \cos\theta_j \sin\phi_j \cos\phi_j \\ 0 & 0 & 0 \\ \sin\theta_j \cos\theta_j \sin\phi_j \cos\phi_j & 0 & 0 \end{pmatrix} \text{ and}$$

$$\boldsymbol{E}_{body-5}=\begin{pmatrix} 0 & 0 & 0 \\ 0 & 0 & \frac{\sin\theta_j \cos 2\phi_j}{2} \\ 0 & \frac{\sin\theta_j \cos 2\phi_j}{2} & 0 \end{pmatrix}.$$

$\boldsymbol{E}_{body-1}$ represents axisymmetric extension flow, as shown in figure 3.7. $\boldsymbol{E}_{body-2}$ represents transverse extensional flow-1, shown on the left in figure 3.8. $\boldsymbol{E}_{body-3}$ represents transverse extensional flow-2, as shown on the right of figure 3.8. $\boldsymbol{E}_{body-4}$ represents longitudinal extensional flow-1 in the x-z plane, as shown on the left in

figure (3.9). And $\boldsymbol{E}_{body-5}$ represents longitudinal extensional flow-2 in y-z plane, as shown on the right in figure (3.9). Let the disturbance velocity due to each of the five above flows be represented as $\boldsymbol{u}_1^1$, $\boldsymbol{u}_2^1$, $\boldsymbol{u}_3^1$, $\boldsymbol{u}_4^1$ and $\boldsymbol{u}_5^1$ respectively.

The expressions for the five disturbance velocity fields with the relevant constants can be found out by using the procedure mentioned in §3.1.3. Summing up these five disturbance velocity fields will give the total disturbance velocity field $\boldsymbol{u}_1^{'}$ due to a spheroidal particle rotating in a simple shear flow. Thus,

$$\boldsymbol{u}_1^{'} = \boldsymbol{u}_1^1 + \boldsymbol{u}_2^1 + \boldsymbol{u}_3^1 + \boldsymbol{u}_4^1 + \boldsymbol{u}_5^1,$$

where,

(1)

$$\boldsymbol{u}_1^1 = A_{axi(shear)} \left( \mathbf{S}_{2,0}^{(3)} \right),$$

$$A_{axi(shear)} = \left( \frac{2d\sqrt{\xi_0^2 - 1}}{(Q_1^1 - \xi_0 Q_2^1)} \right) \left( \frac{\sin^2\theta_j \sin\phi_j \cos\phi_j}{2} \right),$$

(2)

$$\boldsymbol{u}_2^1 = A_{te(shear)}^1 \left( \mathbf{S}_{2,2}^{(3)} + \mathbf{S}_{2,-2}^{(3)} \right),$$

$$A_{te(shear)}^1 = \left( \frac{2d\sqrt{\xi_0^2 - 1}}{(\xi_0 Q_2^1 - 3Q_1^1)} \right) \left( \frac{-\cos^2\theta_j \sin\phi_j \cos\phi_j + \sin\phi_j \cos\phi_j}{2} \right),$$

(3)

$$\boldsymbol{u}_3^1 = A_{te(shear)}^2 \left( \mathbf{S}_{2,2}^{(3)} - \mathbf{S}_{2,-2}^{(3)} \right),$$

$$A_{te(shear)}^2 = \left( \frac{2id\sqrt{\xi_0^2 - 1}}{(3Q_1^1 - \xi_0 Q_2^1)} \right) \left( \frac{\cos\theta_j \cos 2\phi_j}{2} \right),$$

(4)

$$\boldsymbol{u}_4^1 = A_{le(shear)}^1 \left( \mathbf{S}_{2,1}^{(3)} - \mathbf{S}_{2,-1}^{(3)} \right),$$

$$A^1_{le(shear)} = \left(\frac{d(\xi_0^2-1)}{2\xi_0(Q_1^0-\xi_0 Q_2^0)}\right)(\sin\theta_j\cos\theta_j\sin\phi_j\cos\phi_j)\,,$$

and

(5)

$$\boldsymbol{u}_5^1 = A^2_{le(shear)}\left(\mathbf{S}^{(3)}_{2,1}+\mathbf{S}^{(3)}_{2,-1}\right),$$

$$A^2_{le(shear)} = \left(\frac{id(\xi_0^2-1)}{2\xi_0(Q_1^0-\xi_0 Q_2^0)}\right)\left(\frac{\sin\theta_j\cos 2\phi_j}{2}\right).$$

The inertial acceleration in the actual problem due to the disturbance velocity $\boldsymbol{f}$, and non-Newtonian Stress due to the disturbance velocity $\boldsymbol{\sigma}^{(1)}_{NN}$ can be found out once $\boldsymbol{u}_1^{'}$ is known. Now, the $O(Re)$ inertial and $O(De)$ viscoelastic contributions may be determined by calculating the respective volume integrals. The angular velocity, $\boldsymbol{W}_{shear}$, of the neutrally buoyant spheroid placed in a simple shear flow is then determined by solving the first-order differential equation (3.38). As a test case, the Jeffery orbit equations have been derived using the (3.38) by equating the Reynolds and Deborah numbers to zero, and neglecting the inertia of the particle ($St$=0). With the neglect of fluid inertia, viscoelasticity and particle inertia the angular velocity, $\boldsymbol{W}_{shear}$, of the spheroid is given by

$$\boldsymbol{W}_{shear} = \int_{S_p} \boldsymbol{\Gamma}.\boldsymbol{x}.(\boldsymbol{\sigma}^{(2)}.\boldsymbol{n})dS.$$

This surface integral was evaluated using the expressions for the stress field in terms of vector spheroidal harmonics, and yielded the angular velocity of the spheroid in the body fixed coordinate system. We find the following equation for the components of the angular velocity transverse to the axis of symmetry.

$$W_{shear-x} = -\left(\frac{\sin\theta_j}{2} + \frac{\xi_0}{2\sqrt{\xi_0^2-1}}\sin\theta_j\cos 2\phi_j\right) \tag{3.39}$$

$$W_{shear-y} = \left(\frac{\xi_0}{\sqrt{\xi_0^2-1}}\sin\theta_j\cos\theta_j\sin\phi_j\cos\phi_j\right)$$

These have been verified to be identical to the Jeffery orbit equations (3.34) given in the space fixed coordinate system. The equation for the component of the angular velocity along the axis of symmetry is a trivial one, since the particle rotates at a rate commensurate with the projection of the ambient vorticity vector along its axis of symmetry.

CHAPTER 4

# SCOPE FOR THE FUTURE

## Conclusions

Kushch's spheroidal harmonics formalism, together with the use of the generalised reciprocal theorem, is first applied to the sedimentation problem, leading to closed-form analytical expressions for the $O(\mathrm{Re})$ inertial and $O(\mathrm{De})$ viscoelastic torques in sedimentation. The two torques act in opposite directions and by balancing the two we have obtained a neutral curve as a function of De/Re and particle aspect ratio. Despite extensive work on this classic problem, our fully analytical approach shows some of the earlier results to be incorrect. We have shown that Leal's viscoelastic torque acting on the slender fiber is qualitatively right but quantitatively wrong [see Leal (1975)]. Also, Galdi et.al have reported reversal of the viscoelastic torque as the spheroid tends to a fiber for $\epsilon_1 = -1.25, -1.42$ ($\epsilon_1$ is related to the ratio of the normal stress coefficients), this error can be ascribed to the fact that the viscoelastic torque vanishes very rapidly for a slender fiber; a variation that might lead to errors in the numerics [see G.P.Galdi *et al.* (2002)].

In the near future, we intend to complete the calculation of the inertial and viscoelastic contributions to the angular velocity of a neutrally buoyant spheroid in simple shear flow. The simple shear flow problem is inherently more complicated, since the orientation of the spheroid now changes as a function of time even in the inertialess limit (as the particle moves along a Jeffery orbit). Further, unlike sedimentation where the only stable orientations turn out to the transverse and longitudinal ones, the more complicated angular dependencies in simple shear flow

allow, in principle, for the existence of stable intermediate orbits (that is, in between the limits of in-plane tumbling and log-rolling). The results for the simple shear flow are perhaps best understood in the form shown in figure 4.1.

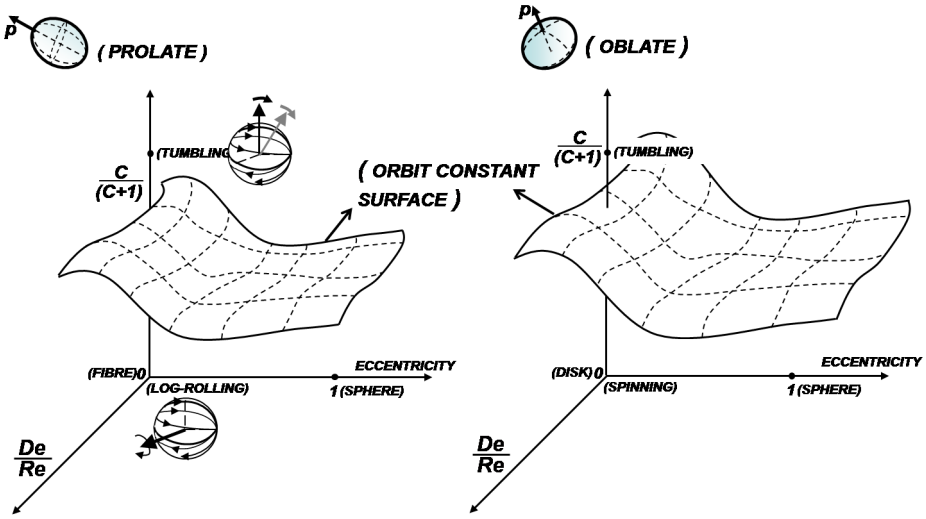


Figure 4.1: Orbit constant surfaces in a simple shear flow

The figure shows an orbit constant surface plotted as a function of the particle aspect ratio and De/Re. This non-trivial surface arises because in the simple shear flow problem one can have intermediate orbits due to competing inertial and viscoelastic effects. On the vertical axis of the figure 4.1 we have the quantity $\frac{C}{C+1}$ that characterizes the orbit in which the spheroid is rotating; $\frac{C}{C+1}$ is equal to zero for a log-rolling motion and is equal to one for a tumbling motion. On the two horizontal axes we have the particle aspect ratio and the ratio De/Re.

We eventually intend to apply Kushch's formalism to find the effect of pair-particle interactions on the orientation distribution across the Jeffery orbits for a particle placed in a simple shear flow. Kushch's formalism, in fact, allows one to model N particle systems. For the said problem, one needs to study the drift across Jeffery orbits of a single test particle as it interacts hydrodynamically with

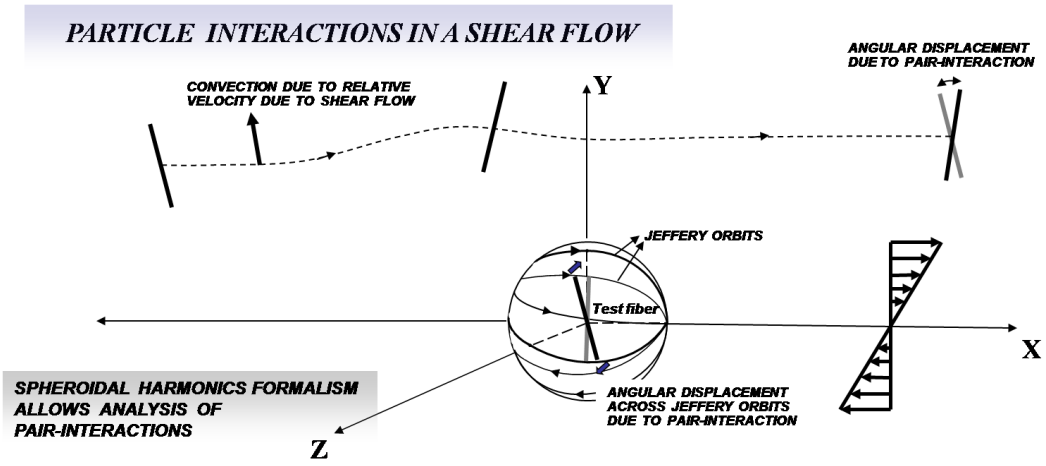


Figure 4.2: Particle interactions in a simple shear flow

the particles that are convected around it due to the externally imposed shear flow [see figure 4.2].

# Appendices

# A Spheroidal coordinate systems

## A.1 Prolate spheroidal coordinate system

In the prolate spheroidal coordinate system, $(\xi, \eta, \phi)$ are related to the Cartesian coordinates (x,y,z) by:

$$x + iy = d\sqrt{\xi^2 - 1}\sqrt{1 - \eta^2}\exp(i\phi), z = d\xi\eta; \tag{A-1}$$

$$1 \leq \xi \leq \infty, |\eta| \leq 1, 0 \leq \phi < 2\pi$$

The unit vector in the prolate spheroidal coordinate system are:
$\widehat{e}_\xi = (\frac{\xi\sqrt{1-\eta^2}\cos\phi}{\sqrt{\xi^2-\eta^2}})\widehat{e}_x + (\frac{\xi\sqrt{1-\eta^2}\sin\phi}{\sqrt{\xi^2-\eta^2}})\widehat{e}_y + (\frac{\eta\sqrt{\xi^2-1}}{\sqrt{\xi^2-\eta^2}})\widehat{e}_z,$
$\widehat{e}_\eta = (\frac{-\eta\sqrt{1-\eta^2}\cos\phi}{\sqrt{\xi^2-\eta^2}})\widehat{e}_x + (\frac{-\eta\sqrt{1-\eta^2}\sin\phi}{\sqrt{\xi^2-\eta^2}})\widehat{e}_y + (\frac{\eta\sqrt{\xi^2-1}}{\sqrt{\xi^2-\eta^2}})\widehat{e}_z,$
$\widehat{e}_\phi = (-\sin\phi)\widehat{e}_x + (\cos\phi)\widehat{e}_y.$

The Cartesian partial derivatives in prolate spheroidal coordinates are:
$\frac{\partial}{\partial x} = (\frac{\xi\sqrt{\xi^2-1}\sqrt{1-\eta^2}\cos\phi}{d(\xi^2-\eta^2)})\frac{\partial}{\partial\xi} - (\frac{\eta\sqrt{\xi^2-1}\sqrt{1-\eta^2}\cos\phi}{d(\xi^2-\eta^2)})\frac{\partial}{\partial\eta} - (\frac{\sin\phi}{d\sqrt{\xi^2-1}\sqrt{1-\eta^2}})\frac{\partial}{\partial\phi},$
$\frac{\partial}{\partial y} = (\frac{\xi\sqrt{\xi^2-1}\sqrt{1-\eta^2}\sin\phi}{d(\xi^2-\eta^2)})\frac{\partial}{\partial\xi} - (\frac{\eta\sqrt{\xi^2-1}\sqrt{1-\eta^2}\sin\phi}{d(\xi^2-\eta^2)})\frac{\partial}{\partial\eta} + (\frac{\cos\phi}{d\sqrt{\xi^2-1}\sqrt{1-\eta^2}})\frac{\partial}{\partial\phi},$
$\frac{\partial}{\partial z} = (\frac{\eta(\xi^2-1)}{d(\xi^2-\eta^2)})\frac{\partial}{\partial\xi} + (\frac{\xi(1-\eta^2)}{d(\xi^2-\eta^2)})\frac{\partial}{\partial\xi}.$

The scale factors in the prolate spheroidal coordinate system are:
$h_\xi = \frac{\sqrt{\xi^2-1}}{d\sqrt{\xi^2-\eta^2}}, \quad h_\eta = \frac{\sqrt{1-\eta^2}}{d\sqrt{\xi^2-\eta^2}}, \quad h_\phi = \frac{1}{d\sqrt{\xi^2-1}\sqrt{1-\eta^2}}.$

The area element and volume elements in an prolate spheroidal coordinate system are

$dA = d^2\sqrt{\xi_0^2 - 1}\sqrt{\xi_0^2 - \eta^2}; \quad dV = d^3\sqrt{\xi^2 - \eta^2}.$

## A.2 Oblate spheroidal coordinate system

In the oblate spheroidal coordinate system, $(\xi, \eta, \phi)$ are related to the Cartesian coordinates (x,y,z) by:

$$x + iy = d\xi\sqrt{1-\eta^2}\exp(i\phi), z = d\sqrt{\xi^2-1}\eta; \tag{A-2}$$

$$1 \leq \xi \leq \infty, |\eta| \leq 1, 0 \leq \phi < 2\pi$$

The unit vector in the oblate spheroidal coordinate system are:

$\widehat{e}_\xi = (\frac{\sqrt{\xi^2-1}\sqrt{1-\eta^2}\cos\phi}{\sqrt{(\xi^2-1)+\eta^2}})\widehat{e}_x + (\frac{\sqrt{\xi^2-1}\sqrt{1-\eta^2}\sin\phi}{\sqrt{(\xi^2-1)+\eta^2}})\widehat{e}_y + (\frac{\xi\eta}{\sqrt{(\xi^2-1)+\eta^2}})\widehat{e}_z,$

$\widehat{e}_\eta = (\frac{-\xi\eta\cos\phi}{\sqrt{(\xi^2-1)+\eta^2}})\widehat{e}_x + (\frac{-\xi\eta\sin\phi}{\sqrt{(\xi^2-1)+\eta^2}})\widehat{e}_y + (\frac{\xi\eta}{\sqrt{(\xi^2-1)+\eta^2}})\widehat{e}_z,$

$\widehat{e}_\phi = (-\sin\phi)\widehat{e}_x + (\cos\phi)\widehat{e}_y.$

The Cartesian partial derivatives in oblate spheroidal coordinates are:

$\frac{\partial}{\partial x} = (\frac{(\xi^2-1)\sqrt{1-\eta^2}\cos\phi}{d((\xi^2-1)+\eta^2)})\frac{\partial}{\partial\xi} - (\frac{\xi\eta\sqrt{1-\eta^2}\cos\phi}{d((\xi^2-1)+\eta^2)})\frac{\partial}{\partial\eta} - (\frac{\sin\phi}{d\xi^2\sqrt{1-\eta^2}})\frac{\partial}{\partial\phi},$

$\frac{\partial}{\partial y} = (\frac{(\xi^2-1)\sqrt{1-\eta^2}\sin\phi}{d((\xi^2-1)+\eta^2)})\frac{\partial}{\partial\xi} - (\frac{\xi\eta\sqrt{1-\eta^2}\sin\phi}{d((\xi^2-1)+\eta^2)})\frac{\partial}{\partial\eta} + (\frac{\cos\phi}{d\xi^2\sqrt{1-\eta^2}})\frac{\partial}{\partial\phi},$

$\frac{\partial}{\partial z} = (\frac{(\xi\eta\sqrt{\xi^2-1}}{d((\xi^2-1)+\eta^2)})\frac{\partial}{\partial\xi} + (\frac{\sqrt{\xi^2-1}(1-\eta^2)}{d((\xi^2-1)+\eta^2)})\frac{\partial}{\partial\eta}.$

The scale factors in the oblate spheroidal coordinate system are:

$h_\xi = \frac{\sqrt{\xi^2-1}}{d\sqrt{(\xi^2-1)+\eta^2}}, \qquad h_\eta = \frac{\sqrt{1-\eta^2}}{d\sqrt{(\xi^2-1)+\eta^2}}, \qquad h_\phi = \frac{1}{d\xi\sqrt{1-\eta^2}}.$

The area element and volume elements in an oblate spheroidal coordinate system are

$dA = d^2\xi_0\sqrt{(\xi_0^2-1)+\eta^2}; \qquad dV = \frac{d^3\big((\xi^2-1)+\eta^2\big)\xi}{\sqrt{\xi^2-1}}.$

All of the above formulae have been derived using the procedures and conven-

tions mentioned in Happel & Brenner (1973).

# B Lorentz reciprocal theorem

The generalised reciprocal theorem relates the velocity and stress fields of two problems, the actual problem $(\boldsymbol{\sigma}^{(1)}, \boldsymbol{u}^{(1)})$ and a test problem $(\boldsymbol{\sigma}^{(2)}, \boldsymbol{u}^{(2)})$ for which the solution is known. Both $(\boldsymbol{\sigma}^{(1)}, \boldsymbol{u}^{(1)})$ and $(\boldsymbol{\sigma}^{(2)}, \boldsymbol{u}^{(2)})$ are solutions of the flow past the same body but with different boundary conditions on the surface of the body and possibly governed by different dynamical equations.

Let the actual problem be a body undergoing a specified motion in a non-Newtonian Fluid. The non-dimensional equation of motion with the mass conservation is as given below:

$$\boldsymbol{\nabla} \cdot \boldsymbol{\sigma}^{(1)} = Re \left( \frac{D\mathbf{u}^{(1)}}{Dt} \right); \tag{B-1}$$

$$\boldsymbol{\nabla}.\mathbf{u}^{(1)} = 0$$

Here, $\boldsymbol{\sigma}^{(1)}$ is the total stress in the non-Newtonian fluid, $Re$ is the Reynolds number and $\mathbf{u}^{(1)}$ is the velocity field of the actual problem.

The total stress of the actual problem is composed of two pieces, the Newtonian stress $\boldsymbol{\sigma}_N^{(1)}$ involving linear velocity gradients and the non-Newtonian stress $\boldsymbol{\sigma}_{NN}^{(1)}$ involving non-linear velocity gradients.

$$\boldsymbol{\sigma}^{(1)} = \boldsymbol{\sigma}_N^{(1)} + De \left( \boldsymbol{\sigma}_{NN}^{(1)} \right) \tag{B-2}$$

The non-dimensional Newtonian stress of the actual problem can be written as:

$$\boldsymbol{\sigma}_{Nij}^{(1)} = -p^{(1)} \boldsymbol{\delta}_{ij} + 2\boldsymbol{E}_{ij}^{(1)}; \tag{B-3}$$

where $p^{(1)}$ is the pressure and $\boldsymbol{E}_{ij}^{(1)}$ is the strain rate tensor of the actual problem.

The non-dimensionalised non-Newtonian stress is composed of two parts:

$$\boldsymbol{\sigma}^{(1)}_{NN} = \boldsymbol{\sigma}^{(1)}_{NNC} + \boldsymbol{\sigma}^{(1)}_{NNQ} \tag{B-4}$$

The first component involving the corotational derivative of the rate of strain can be written as:

$$\boldsymbol{\sigma}^{(1)}_{NNC} = 2\epsilon \left( \frac{\partial \boldsymbol{E}}{\partial t} + \boldsymbol{\nabla .} \left( \boldsymbol{uE} \right) + \left( \boldsymbol{W.E} \right) + \left( \boldsymbol{W.E} \right)^{t} \right)$$

and the second contribution that is quadratic in the rate of strain can be written as:

$$\boldsymbol{\sigma}^{(1)}_{NNQ} = 4(1+\epsilon)\boldsymbol{E.E}$$

where $De$ is the Deborah number, $\boldsymbol{E} = 1/2(\boldsymbol{\nabla u} + \boldsymbol{\nabla u^t})$ is the strain rate tensor, $\boldsymbol{W} = 1/2(\boldsymbol{\nabla u} - \boldsymbol{\nabla u^t})$ is the vorticity tensor and $\epsilon$ is an intrinsic fluid property.

Equation of motion of the test problem, which belongs to the Stokes regime are:

$$\boldsymbol{\nabla .} \boldsymbol{\sigma}^{(2)} = 0 \tag{B-5}$$

$$\boldsymbol{\nabla} . \mathbf{u}^{(2)} = 0$$

The non-dimensionalised Newtonian stress of the test problem can be written as:

$$\boldsymbol{\sigma}_{ij}{}^{(2)} = -p^{(2)}\boldsymbol{\delta}_{ij} + 2\boldsymbol{E}^{(2)}_{ij}; \tag{B-6}$$

where $p^{(2)}$ is the pressure and $\boldsymbol{E}^{(2)}_{ij}$ is the strain rate tensor of the test problem.

By double doting equation (B-2) by $\boldsymbol{E}^{(2)}_{ij}$ and equation (B-6) by $\boldsymbol{E}^{(1)}_{ij}$ and making use of equation (B-3), We arrive at the following result:

$$2\boldsymbol{E}^{(1)} : \boldsymbol{E}^{(2)} \Rightarrow \boldsymbol{\sigma}^{(1)} : \boldsymbol{E}^{(2)} - De\left(\boldsymbol{\sigma}_{NN}^{(1)} : \boldsymbol{E}^{(2)}\right) = \boldsymbol{\sigma}^{(2)} : \boldsymbol{E}^{(1)}; \tag{B-7}$$

Since $\boldsymbol{E}_{ij} = \boldsymbol{E}_{ji}$

Using $\boldsymbol{\sigma} : \boldsymbol{E} \Rightarrow \boldsymbol{\sigma} : \boldsymbol{\nabla u} = \boldsymbol{\nabla .}\left(\boldsymbol{u.\sigma}\right) - \boldsymbol{u.}\left(\boldsymbol{\nabla .\sigma}\right)$ equation (B-7) can be written as:

$$\boldsymbol{\sigma}^{(1)} : \boldsymbol{\nabla u}^{(2)} - \boldsymbol{\sigma}^{(2)} : \boldsymbol{\nabla u}^{(1)} = De\left(\boldsymbol{\sigma}_{NN}^{(1)} : \boldsymbol{\nabla u}^{(2)}\right) \tag{B-8}$$

Further simplification leads to:

$$\boldsymbol{\nabla}.\left(\boldsymbol{u}^{(2)}.\boldsymbol{\sigma}^{(1)}\right) - \boldsymbol{\nabla}.\left(\boldsymbol{u}^{(1)}.\boldsymbol{\sigma}^{(2)}\right) = \left(\boldsymbol{\nabla}.\boldsymbol{\sigma}^{(1)}\right).\boldsymbol{u}^{(2)} + De\left(\boldsymbol{\sigma}_{NN}^{(1)} : \boldsymbol{\nabla u}^{(2)}\right); \left\{\boldsymbol{\nabla}.\boldsymbol{\sigma}^{(2)} = 0\right\} \tag{B-9}$$

Integrating the above equation (B-9) over the entire volume of the fluid and using the Gauss divergence theorem,we get:

$$\int_V \left(\boldsymbol{n}.\left(\boldsymbol{u}^{(2)}.\boldsymbol{\sigma}^{(1)}\right) - \boldsymbol{n}.\left(\boldsymbol{u}^{(1)}.\boldsymbol{\sigma}^{(2)}\right)\right) dS = \int_V \left(Re\left(\frac{D\boldsymbol{u}^{(1)}}{Dt}\right).\boldsymbol{u}^{(2)} + De\left(\boldsymbol{\sigma}_{NN}^{(1)} : \boldsymbol{\nabla u}^{(2)}\right)\right) dV \tag{B-10}$$

# C Relation between partial vectorial solutions of the Stokes equation in spheroidal and spherical coordinate system

The following is the set of the partial vectorial solutions of Stokes equation in the spheroidal coordinate system: constrained at $\|\mathbf{r}\| \to \infty$, or singular $\mathbf{S}_{ts}^{(i)} = \mathbf{S}_{ts}^{(i)}(\mathbf{r},\ d)$:

$$\begin{aligned}
\mathbf{S}_{ts}^{(1)} &= \mathbf{e}_1 F_{t+1}^{s-1} - \mathbf{e}_2 F_{t+1}^{s+1} + \mathbf{e}_3 F_{t+1}^{s}; \qquad \text{(C-1)}\\
\mathbf{S}_{ts}^{(2)} &= \frac{1}{t}\left[\mathbf{e}_1(t+s)F_t^{s-1} + \mathbf{e}_2(t-s)F_t^{s+1} + \mathbf{e}_3 s F_t^{s}\right];\\
\mathbf{S}_{ts}^{(3)} &= \mathbf{e}_1\left\{-(x-iy)\mathrm{D}_2 F_{t-1}^{s-1} - \left[\left(\xi^{(0)}\right)^2 - 1\right] d\mathrm{D}_1 F_t^s + (t+s-1)(t+s)\beta_{-(t+1)}F_{t-1}^{s-1}\right\}\\
&\quad + \mathbf{e}_2\left\{(x+iy)\mathrm{D}_1 F_{t-1}^{s+1} - \left[\left(\xi^{(0)}\right)^2 - 1\right] d\mathrm{D}_2 F_t^s - (t-s-1)(t-s)\beta_{-(t+1)}F_{t-1}^{s+1}\right\}\\
&\quad + \mathbf{e}_3\left[z\mathrm{D}_3 F_{t-1}^s - \left(\xi^{(0)}\right)^2 d\mathrm{D}_3 F_t^s + C_{-(t+1),s}F_{t-1}^s\right];
\end{aligned}$$

We give some idea of a limiting behavior of the above vectorial solutions of Stokes equations. So, in the case where a spheroid degenerates into a sphere ($d \to 0$ and $\xi \to \infty$ so that $d\xi \to r,\ \eta \to \cos\theta$ in (C1)), we have the following limiting relations

$$\lim_{d\to 0}\left(\frac{2}{d}\right)^{t+3-i}\mathbf{S}_{ts}^{(i)}(\mathbf{r},\ d) = \frac{(-1)^s\sqrt{\pi}}{\Gamma(t-i+7/2)}\left[\mathbf{U}_{ts}^{(i)}(\mathbf{r}) + \delta_{i3}\frac{r^2}{(2k+1)}\mathbf{U}_{ts}^{(1)}(\mathbf{r})\right]; \qquad \text{(C-2)}$$

The functions $\mathbf{U}_{t,s}^{(i)}$ are the singular vectorial solutions of Stokes equation in the

spherical basis, of the following form

$$\begin{aligned}
\mathbf{U}_{ts}^{(1)} &= \frac{(t-s)!}{r^{t+2}}\left(-(t+1)\mathbf{P}_{ts}^{(1)}+\mathbf{P}_{ts}^{(2)}\right); \quad \mathbf{U}_{ts}^{(2)}=\frac{(t-s)!}{r^{t+1}}\mathbf{P}_{ts}^{(3)};\\
\mathbf{U}_{ts}^{(3)} &= \frac{(t-s)!}{r^{t}}\left(\gamma_{-t-1}\mathbf{P}_{ts}^{(1)}+\beta_{-t-1}\mathbf{P}_{ts}^{(2)}\right);
\end{aligned}$$

where $\gamma_t = \frac{t}{2t+3}$ and $\mathbf{P}_{ts}^{(i)}$ are the vectorial spherical harmonics (Morse & Feshbach 1953):

$$\begin{aligned}
\mathbf{P}_{ts}^{(1)} &= \mathbf{e}_r Y_t^s(\theta,\varphi); \qquad \text{(C-3)}\\
\mathbf{P}_{ts}^{(2)} &= \mathbf{e}_\theta \frac{\partial}{\partial\theta}Y_t^s(\theta,\varphi)+\frac{\mathbf{e}_\varphi}{\sin\theta}\frac{\partial}{\partial\varphi}Y_t^s(\theta,\varphi);\\
\mathbf{P}_{ts}^{(3)} &= \frac{\mathbf{e}_\theta}{\sin\theta}\frac{\partial}{\partial\varphi}Y_t^s(\theta,\varphi)-\mathbf{e}_\varphi\frac{\partial}{\partial\theta}Y_t^s(\theta,\varphi).
\end{aligned}$$

The functions (C3) are the linear combinations of the functions introduced elsewhere (e.g., Kim & Karilla 1991). As easy to show, at $r\to\infty$ the functions $\mathbf{U}_{1s}^{(3)}\sim 1/r$; for the rest of singular solutions $\mathbf{U}_{ts}^{(i)}$ the decay rate is higher. It is fairly straightforward to show that the same limiting behavior show the functions $\mathbf{S}_{ts}^{(i)}$ at $r\to\infty$ and $d$ being fixed.

# References


Bartman, E., Goldsmith, H. & Mason, S. 1975 Particle motions in non-newtonian media, iii. further observations in elasticoviscous fluids. *Rheol. Acta* **14**, 776–782.

Batchelor, G. K. 1970 Slender-body theory for particles of arbitrary cross-section in stokes flow. *J. Fluid Mech.* **44**, 791810.

Batchelor, G. K. 1972 Sedimentation in a dillute dispersion of spheres. *J. Fluid Mech.* **52**, 245268.

Bird, R. B., Armstrong, R. C. & Hassager, O. 1987 Dynamics of polymeric liquids, volume-1. *John Wiley and Sons* .

Chwang, A. T. & Wu, T. Y.-T. 1975 Hydromechanics of low-reynolds-number flow.part 2. singularity method for stokes flows. *J. Fluid Mech.* **67**, 787–815.

Cox, R. G. 1965 The steady motion of a particle of arbitrary shape at small reynolds numbers. *J. Fluid Mech.* **23**, 625–643.

Cox, R. G. 1970 The motion of long slender bodies in a viscous fluid part 1. general theory. *J. Fluid Mech.* **44**, 791–810.

Cox, R. G. 1989 Inertia effects on the motion of long slender bodies. *J. Fluid Mech.* **209**, 435–462.

Feng, J., D.Joseph, D., Glowinski, R. & W.Pan, T. 1995 A three-dimensional computation of the force and torque on a ellipsoid settling slowly through a viscoelastic fluid. *J. Fluid Mech.* **283**, 1–16.

G.P.Galdi, A.Vaidya, Pokorny, M., Daniel, D. J. & Feng, J. 2002 Orientation of symmetric bodies falling in a second-order liquid at non-zero reynolds number. *Mathematical Models and Methods in Applied Sciences* **12**, 1653–1690.

Happel, J. & Brenner, H. 1973 Low reynolds number hydrodynamics. *Noordhoff International* .

Jeffery, G. B. 1922 The motion of ellipsoidal particles immersed in a viscous fluid. *Proc. Roy . Soc. Lon.* **102**, 161–179.

K.Chiba, Song, K.-W. & A.Horikawa 1986 Motion of a slender body in quiescent polymer solutions. *Rheologica Acta* **25**, 380–388.

Kim, S. & Karrila, S. J. 1991 Microhydrodynamics: Principles and selected applications. *Butterworth-Heinemann* .

Koch, D. L. & Shaqfeh, E. S. 1989 The instability of a dispersion of sedimenting spheroids. *J. Fluid Mech.* **209**, 521–542.

Kushch, V. I. 1997 Microstresses and effective elastic moduli of a solid reinforced by periodically distributed spheroidal particles. *Int J. of Solid Structures* .

Kushch, V. I. & Sangani, A. S. 2003 The complete solutions for stokes interactions of spheroidal particles by the mutipole expansion method. *Preprint, Int J. of Mutiphase Flow.* **34**, 1353–1366.

Lamb, S. H. 1932 Hydrodynamics. *Cambridge Mathematical Library* .

Larson, R. G. 1988 Constitutive equations for polymer melts and solutions. *Butterworths* .

Leal, L. G. 1975 The slow motion of slender rod-like particles in a second-order fluid. *J. Fluid Mech.* **69**, 305–337.

Leal, L. G. 1980 Particle motions in a viscous fluid. *Ann. Rev. Fluid Mech.* **12**, 435–76.

Morse, P. M. & Feshbach, H. 1953 Methods of theoretical physics. *McGraw-Hill book company, Inc* .

Sangani, A. S. & Mo, G. 1996 An $O$(n) algorithm for stokes and laplace interactions of particles. *Phys. Fluids* .

Shatz, L. F. 2004 Singularity method for oblate and prolate spheroids in stokes and linearized oscillatory flow. *Physics of fluids* **16**, 664–677.

Subramanian, G. & Koch, D. L. 2005 Inertial effects on fibre motion in simple shear flow. *J. Fluid Mech.* **535**, 383–414.

Subramanian, G. & Koch, D. L. 2006 Inertial effects on the orientation of nearly spherical particles in simple shear flow. *J. Fluid Mech.* **557**, 257–296.

T.Chwang, A. & Wu, T.-T. 1974 Hydromechanics of low-reynolds-number flow.part 1. rotation of axisymmetric prolate bodies. *J. Fluid Mech.* **63**, 607–622.